



## A synthesis of hourly and daily precipitation extremes in different climatic regions

Renaud Barbero, Hayley Fowler, Stephen Blenkinsop, Seth Westra, Vincent Moron, Elizabeth Lewis, Steven Chan, Geert Lenderink, Elizabeth Kendon, Selma Guerreiro, et al.

### ► To cite this version:

Renaud Barbero, Hayley Fowler, Stephen Blenkinsop, Seth Westra, Vincent Moron, et al.. A synthesis of hourly and daily precipitation extremes in different climatic regions. *Weather and Climate Extremes*, 2019, 26, pp.1-20. 10.1016/j.wace.2019.100219 . hal-02464970

**HAL Id: hal-02464970**

**<https://hal.science/hal-02464970>**

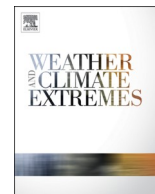
Submitted on 16 May 2020

**HAL** is a multi-disciplinary open access archive for the deposit and dissemination of scientific research documents, whether they are published or not. The documents may come from teaching and research institutions in France or abroad, or from public or private research centers.

L'archive ouverte pluridisciplinaire **HAL**, est destinée au dépôt et à la diffusion de documents scientifiques de niveau recherche, publiés ou non, émanant des établissements d'enseignement et de recherche français ou étrangers, des laboratoires publics ou privés.



Distributed under a Creative Commons Attribution - NonCommercial - NoDerivatives 4.0 International License



# A synthesis of hourly and daily precipitation extremes in different climatic regions

Renaud Barbero<sup>a,\*</sup>, Hayley J. Fowler<sup>b</sup>, Stephen Blenkinsop<sup>b</sup>, Seth Westra<sup>c</sup>, Vincent Moron<sup>d</sup>, Elizabeth Lewis<sup>b</sup>, Steven Chan<sup>b</sup>, Geert Lenderink<sup>e</sup>, Elizabeth Kendon<sup>f</sup>, Selma Guerreiro<sup>b</sup>, Xiao-Feng Li<sup>b</sup>, Roberto Villalobos<sup>b</sup>, Haider Ali<sup>b</sup>, Vimal Mishra<sup>g</sup>

<sup>a</sup> National Research Institute of Science and Technology for Environment and Agriculture, Mediterranean Ecosystems and Risks, Aix-en-Provence, France

<sup>b</sup> School of Engineering, Newcastle University, Newcastle-upon-Tyne, UK

<sup>c</sup> Faculty of Engineering, Computer and Mathematical Sciences, University of Adelaide, Adelaide, Australia

<sup>d</sup> Aix Marseille Univ, CNRS, IRD, INRA, Coll. de France, CEREGE, Aix en Provence, France

<sup>e</sup> Royal Netherlands Meteorological Institute, De Bilt, the Netherlands

<sup>f</sup> Met Office Hadley Centre, Exeter, UK

<sup>g</sup> Civil Engineering, Indian Institute of Technology, Gandhinagar, India

## ARTICLE INFO

### Keywords:

Hourly precipitation  
Daily precipitation  
Precipitation intensity  
Precipitation duration  
Seasonal cycle  
Diurnal cycle  
CAPE

## ABSTRACT

Climatological features of observed annual maximum hourly precipitation have not been documented systematically compared to those on daily timescales due to observational limitations. Drawing from a quality-controlled database of hourly records sampling different climatic regions including the United States, Australia, the British Isles, Japan, India and peninsular Malaysia over the 1950–2016 period, we examined climatological features of annual maximum precipitation (AMP) across timescales ranging from 1-hr (AMP<sub>1-hr</sub>) to 24-hr (AMP<sub>24-hr</sub>). Our analysis reveals strong relations between the magnitude of AMP and the climatological average annual precipitation (AAP), with geographic variations in the magnitude of AMP<sub>24-hr</sub> across topographic gradients not evident in AMP<sub>1-hr</sub>. Most AMP<sub>1-hr</sub> are found to be embedded within short-duration storms (>70% of AMP<sub>1-hr</sub> are embedded within 1–5 h storms), especially in regions with low AAP and in the tropical zone. Likewise, most AMP<sub>24-hr</sub> are found to be the accumulation of a very limited number of wet hours in the 24-h period (>80% of AMP<sub>24-hr</sub> are due to storms lasting <15 h) across many parts of the sampled regions, highlighting the added-value of hourly data in estimating the actual precipitation intensities. The seasonal distribution of AMP may change across different timescales at a specific location, reflecting the prevalence of different seasonal triggering mechanisms. We also find that most AMP<sub>1-hr</sub> occur preferentially in late afternoon to late evening, slightly later than the usual mid-to-late afternoon peak in the mean precipitation intensity. Finally, analysis of atmospheric instability, realized through the convection available potential energy (CAPE), reveals that CAPE is higher before AMP<sub>1-hr</sub> with respect to AMP<sub>24-hr</sub>, although the response of precipitation intensity seems to saturate at higher CAPE levels, a feature evident both in the tropical and extratropical zones. This study provides insights on climatological features of hourly precipitation extremes and how they contrast with the daily extremes examined in most studies.

## 1. Introduction

Precipitation extremes have received much attention in recent years due to the large impacts they impose on society and their potential intensification in a warmer climate (Trenberth et al., 2003; Bao et al., 2017; Pfahl et al., 2017). Extensive research has examined the dependency of precipitation intensity on surface temperature or dew point

temperature, and observational studies have shown that the intensities of sub-daily precipitation extremes are even more sensitive to changes in temperature compared with those on a daily timescale (Westra et al., 2014; Ivancic and Shaw, 2016; Schroeder and Kirchengast, 2017; Ali and Mishra, 2018), with temperature-extreme precipitation scaling sometimes exceeding that of Clausius-Clapeyron (CC): so-called super-CC scaling (Lenderink and van Meijgaard, 2008; Berg et al., 2013; Loriaux

\* Corresponding author.

E-mail address: [renaud.barbero@irstea.fr](mailto:renaud.barbero@irstea.fr) (R. Barbero).

<https://doi.org/10.1016/j.wace.2019.100219>

Received 17 May 2019; Received in revised form 12 July 2019; Accepted 20 August 2019

Available online 30 August 2019

2212-0947/© 2019 The Authors.

Published by Elsevier B.V. This is an open access article under the CC BY-NC-ND license

(<http://creativecommons.org/licenses/by-nc-nd/4.0/>).

et al., 2017; Lenderink et al., 2017). Additionally, widespread long-term increases in the magnitude of hourly precipitation extremes have been documented across parts of the world, including China (Xiao et al., 2016), the United States (Barbero et al., 2017) and Australia (Guerreiro et al., 2018), with recent convection-permitting climate model simulations projecting a continued intensification into the future due to anthropogenic climate change (Prein et al., 2016, 2017a; Kendon et al., 2017). A recent convection-permitting simulation in the United Kingdom also suggests that the signal of change due to global warming is likely to emerge in shorter-duration precipitation extremes first (Kendon et al., 2018).

Records at hourly resolution may thus be more suitable for examining precipitation extremes as they provide a better picture of the intermittent nature of precipitation (Trenberth et al., 2017) and reflect the timescale on which convective storms operate and initiate short-duration precipitation extremes which are primarily responsible for flash floods in fast responding catchments (Doswell et al., 1996; Brooks and Stensrud, 2000). However, climatological features of hourly precipitation extremes have not been documented systematically across different climate zones due to observational limitations (Lewis et al., 2019) and have not been systematically compared with precipitation extremes on the daily timescales which are used in most studies. For instance, the duration of storms triggering hourly precipitation extremes or the number of wet hours contributing to daily extremes has received little attention. Likewise, the extent to which these events overlap (i.e. concurrent intensity) and how they relate to average annual precipitation has been little studied globally, including in regional analyses.

Whereas mesoscale or isolated convective systems in the mid-latitudes have been shown to initiate intense precipitation on short durations down to a few minutes during the warm season (Prein et al., 2017b), large-scale systems in the cool season are commonly thought to produce less intense but longer-lasting precipitation and to contribute mostly to precipitation extremes on daily or longer timescales (Lamjiri et al., 2017). By contrast, other studies have shown that large-scale systems may also contribute considerably to extreme precipitation on sub-daily timescales across parts of the world (Luo et al., 2016; Utsumi et al., 2017; Barbero et al., 2018). The season during which extreme precipitation intensities take place may thus vary across different durations at a specific site (Zheng et al., 2015). Likewise, hourly precipitation intensities over land are also often locked into the diurnal cycle, with the highest intensities observed, in most cases, in late afternoon at least in midlatitude regions during the warm season when precipitation is related to small-scale thermodynamic processes affecting surface temperature and vertical static stability (Dai and Trenberth, 2004; Evans and Westra, 2012). Precipitation intensities have also been shown to peak at different times of the day due to other factors such as weather types (Moron et al., 2019), topographical conditions (Li, 2017), propagation of moist convection (Ploshay and Lau, 2010) or coastal effects (Kikuchi and Wang, 2008). Examining the diurnal and seasonal timing of precipitation extremes across different timescales may provide more insights into the roles of different climate drivers in producing these extremes.

While climate models may be useful to characterize precipitation globally, a general criticism is that they are not able to explicitly simulate the small-scale convective processes initiating short-duration precipitation extremes (Dai and Trenberth, 2004; Trenberth et al., 2017; Yuan et al., 2013; Cortés-Hernández et al., 2016; Yuan et al., 2013, 2013; Covey et al., 2016; Beranova et al., 2017; Prein et al., 2015; Mooney et al., 2017). Large improvements have been found recently for convection-permitting models (Kendon et al., 2017; Fossler et al., 2014; Prein et al., 2017b) but such simulations are generally very computationally expensive and can only be executed across limited regions and short time periods. Alternatively, satellite observations could be used to provide an estimate of sub-daily precipitation extremes with global coverage but only at the time of the satellite overpass (Hur et al., 2016) and with a spatial resolution that is often too coarse to explicitly detect

small-scale processes conducive to short-lived precipitation extremes. Perhaps most importantly, inferring hourly precipitation amounts from remote sensing is not an easy task and satellite estimates may thus lack credibility for the analysis of precipitation extremes, although data merging exploiting the complementary strengths of gauge, satellite and reanalysis-based precipitation estimates (Beck et al., 2017) are very promising.

The observational surface gauge network provides a direct measure of precipitation and, although the data is generally available with limited coverage and is also subject to systematic measurements errors and inhomogeneities (Blenkinsop et al., 2017), usually describes more realistically sub-daily precipitation variability and extremes. Unfortunately, the lack of sub-daily data sharing across the world has left the research community with little data over limited geographical regions (Zhang et al., 2017), thus hampering global or multi-continental analyses. To bridge this gap, a Global Sub-Daily Rainfall (GSDR) dataset has recently been compiled (Lewis et al., 2019) from multiple data sources in an international initiative under the Global Water and Energy Exchanges (GEWEX) Hydroclimatology Panel INTENSE project (Blenkinsop et al., 2018).

We here examine the climatological features of hourly precipitation extremes in different climatic regions using the GSDR dataset to identify potential universal behaviors. We also examine how they compare to precipitation extremes on daily timescales to highlight the potential added-value of hourly data. Specifically, we sought to establish: 1) how hourly and daily precipitation extremes relate to the climatological average annual precipitation, 2) the proportion of hourly precipitation extremes embedded within daily precipitation extremes, 3) how long are storms producing hourly precipitation extremes and how many wet hours are responsible for daily extremes, 4) the seasonal and diurnal distribution of hourly precipitation conducive to hourly and daily precipitation extremes, and 5) how hourly and daily precipitation extremes relate to the convection available potential energy (CAPE) to better elucidate the role of atmospheric stability in triggering these extreme events. This study can therefore help in defining the climatological features of precipitation extremes from hourly to daily timescales and provide a better understanding of processes which could then be evaluated in numerical models (Cortés-Hernández et al., 2016).

## 2. Data and methods

### 2.1. Global Sub-Daily Rainfall

The Global Sub-Daily Rainfall (GSDR) dataset used in this analysis has been constructed from multiple sources (Lewis et al., 2019) including records from the United States (US), Australia, the British Isles, Japan, India and peninsular Malaysia. We focused on these regions as they provide long and high quality records needed to derive robust statistics and have been extensively used in national studies in the US (Barbero et al., 2017; Canel and Katz, 2018), the United Kingdom (Blenkinsop et al., 2017; Darwish et al., 2018), Australia (Guerreiro et al., 2018; Westra and Sisson, 2011), Japan (Utsumi et al., 2011), Malaysia (Syafarina et al., 2015) and India (Ali and Mishra, 2018). Moreover, these macro-regions encompass large latitudinal and topographic gradients from tropical to midlatitude areas, sampling different climate zones over a large spectrum of climatological average annual precipitation (Fig. 1). We only use gauges with at least 20 years of data and less than 20% missing hours in any given year, which does not exclude potential extended interruptions in the time series at some sites. Overall, the number of records meeting completeness criteria grows with time from 1 690 station records in 1951 to 3559 records in 1992, and then slightly decreases for the most recent years (except in Japan and Malaysia (Fig. S1)) to 1 572 records in 2010. Although the coverage provided by this dataset is not uniform in either space or time and represents an ongoing effort by the international community, the GSDR still represents the most complete direct measurements of hourly

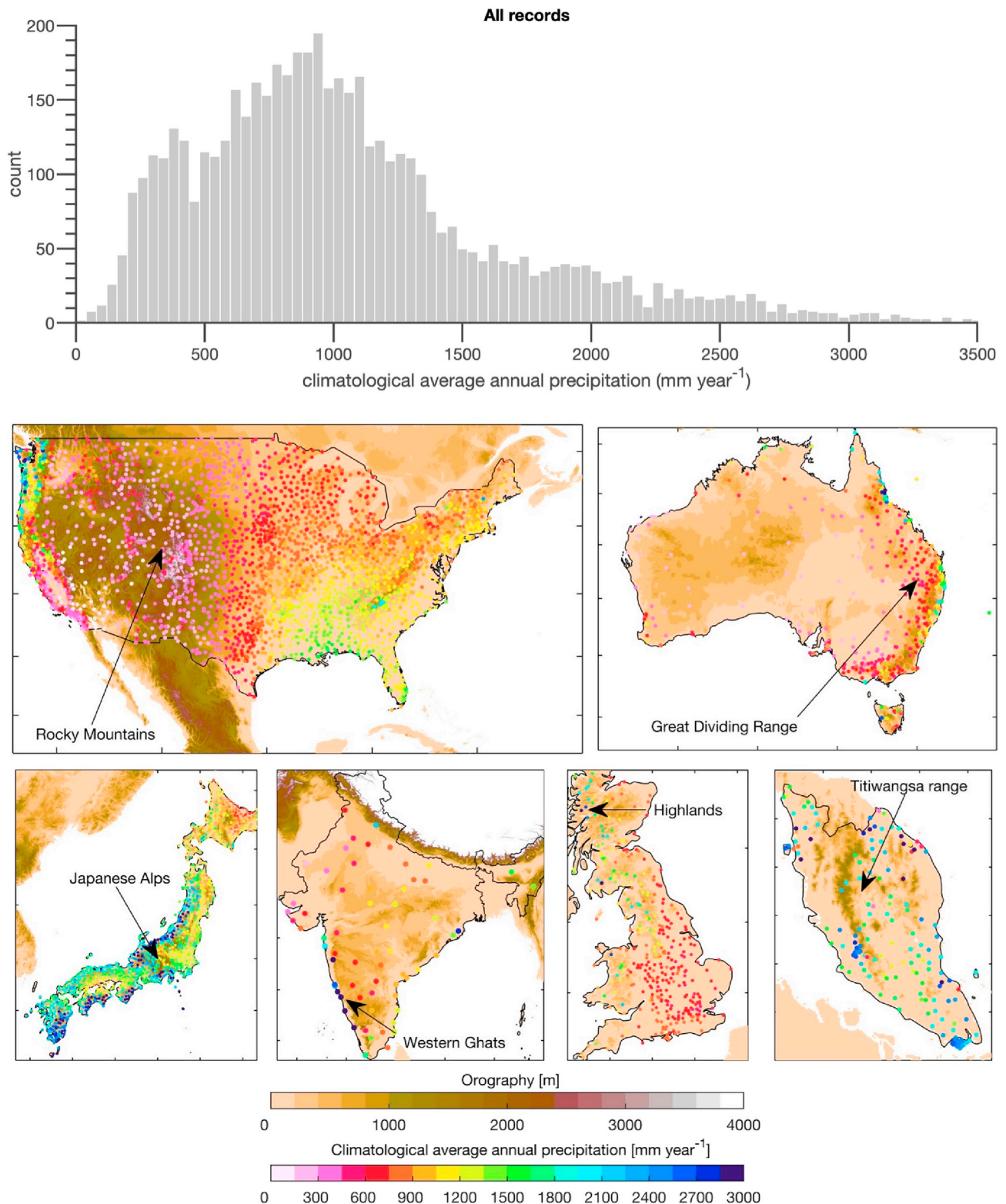


**Fig. 1.** Top) Number of hourly records as a function of the climatological average annual precipitation (AAP) across all regions investigated in this study. Bottom) Orography (meters) alongside climatological average annual precipitation.

precipitation presently available (Lewis et al., 2019).

All data classified as suspect according to pre-existing quality-control flags were treated as missing. Hourly measurements were aggregated up to 3-h, 6-h, 12-h and 24-h using fixed intervals (e.g. 0 000–0300, 0 300–0600, for 3-h data; 0 000–0600, 0 600–1200, for 6-h data and so on) relative to local time (i.e. daily accumulation are calculated from

midnight to midnight). In the following, we only report results for 1-hr and 24-hr as analyses of intermediate durations only show a transition between the characteristics shown at 1-h and 24-hr (not shown).



## 2.2. Annual maximum precipitation

We focus on annual (Jan–Dec) maximum precipitation across various resolutions ranging from 1-h ( $AMP_{1-hr}$ ) to 24-h ( $AMP_{24-hr}$ ). This simple block maxima approach is often used in hydrology to produce estimates of return periods with the advantage that the observations are independent and identically distributed. Note here that the use of moving windows rather than a midnight-to-midnight accumulation would yield better estimates of the size of 24-h events as AMP values were found to be on average  $\sim 1.15$  times higher when considering moving windows compared to fixed windows (Boughton and Jakob, 2017; Morbidelli et al., 2017). However, given that this procedure cannot be applied to 1-h events whose precipitation depth is constrained by the fixed intervals of measurements, we decided to use fixed intervals for a fair comparison across durations. For each gauge we estimate the return levels of AMP across various resolutions ranging from 1-h to 24-h using a generalized extreme value distribution fitted with the maximum likelihood estimator (Katz et al., 2002) under the assumption of a stationary climate. This assumption is obviously questionable in the global warming context and is likely to cause an underestimation of today's return levels in AMP across many regions of the world. However, this study does not seek to examine potential non-stationarity in precipitation extremes but only climatological features across timescales.

## 2.3. Annual maxima characteristics

Separately, we examine three statistics:

1. We calculate the percent of  $AMP_{1-hr}$  that are embedded within  $AMP_{24-hr}$  events (referred hereafter to as concurrent intensity) using a 1-day padding tolerance. In other words, an  $AMP_{1-hr}$  event is included as embedded if it is within 1-day of a  $AMP_{24-hr}$ . The 1-day padding may seem generous but the use of fixed intervals (i.e. 0 000–2 400 for  $AMP_{24-hr}$ ) is expected to decrease the probability of embedding. The 1-day padding enables us to relate  $AMP_{1-hr}$  and  $AMP_{24-hr}$  separated by a few hours (and thus belonging to the same meteorological event) but taking place on two consecutive days.
2. We report on the duration of storms triggering  $AMP_{1-hr}$  and the number of wet hours contributing to  $AMP_{24-hr}$ . The duration is defined here as the length of time from precipitation initiation (any hour  $\geq 1$  mm) to precipitation cessation and does not include any period of dry hours. Note that changes in the resolution of measurements (from 0.25 to 2.5 mm) were observed in the US at some stations (Groisman et al., 2012; Barbero et al., 2017), resulting in both spatial and temporal inhomogeneities, as storm duration is likely to be underestimated at stations measuring precipitation at a coarser resolution. However, this inhomogeneity is minimized through the use of the 1 mm threshold and is not expected to introduce any systematic geographic bias as changes in the bucket size are randomly distributed in space (not shown). This inhomogeneity is rather expected to affect temporal analyses which are not addressed in this study.
3. We estimate the contribution of  $AMP_{1-hr}$  to the corresponding total 24-hr accumulation (referred hereafter to as  $\frac{AMP_{1-hr}}{P_{24-hr}} 100$ ) as an indicator of triggering mechanisms (Blenkinsop et al., 2017).

## 2.4. Dependency on climatological average annual precipitation

All the aforementioned statistics are computed at the site level and then averaged along a climatological average annual precipitation (AAP) gradient (Fig. 1, top). Note that AAP is by no means a universal metric of surface dryness or wetness, which is dependent on additional variables such as temperature and evaporation (Sippel et al., 2017), but simply reflects how much precipitation reaches the surface on average on a yearly basis. Recording sites were pooled together using a binning

method along the AAP gradient using moving 500 mm year<sup>-1</sup> bins, in order to gather a decent number of records along the AAP gradient (Fig. 1, top). The spatial average of the aforementioned statistics within each bin was weighted by the mean distance between one record and the remaining ones, so that less weight was given to the most densely monitored regions following Moron et al. (2019). The 95% confidence intervals of the composite means were computed using 1 000 bootstrapped datasets with replacement sampling at random 50% of the records in a given bin. The 2.5th and 97.5th percentiles of the composite means from the bootstrapped dataset were then used to derive an envelope of confidence.

## 2.5. Tropical versus extra-tropical zones

We also investigate the aforementioned statistics for the tropical and extra-tropical zones separately. The tropical zone is defined here as the region equatorward of 25° latitude.

## 2.6. Seasonal distribution of AMP

Amplitude and phase of climate cycles are generally examined through harmonic analyses (Dai and Trenberth, 2004; Wu et al., 2017). Here, we analyzed the seasonality of AMP across timescales by considering first the modal month during which most AMP take place, and second the fractional distribution of months during which they occur. Whereas the modal month indicates when the AMP is most likely to take place, the fractional distribution provides insights into how uniformly distributed AMP are across the year. The fractional distribution of AMP across the year was measured through the Gini coefficient, an index that has recently been used in hydroclimate studies (Masaki et al., 2014; Rajah et al., 2014). For each record, the frequency of AMP occurrence was computed for each month of the year, sorted by ascending order, summed cumulatively and then converted into a proportion of time expressed by  $y_i (i = 1, \dots, n)$  with  $n = 12$ . The Gini coefficient  $G$  is defined as

$$G = \frac{1}{n} \left( n + 1 - 2 \left( \frac{\sum_{i=1}^n (n+1-i)y_i}{\sum_{i=1}^n y_i} \right) \right)$$

The coefficient ranges within [0,1]. If  $G = 0$ , the frequency of AMP is constant throughout the year without any monthly variation (uniform distribution of frequencies). If  $G = 1$ , all AMP occur during one month of the year with no occurrences for the rest of the year. The Gini coefficient,  $G$ , was calculated for each gauge using all years available which met the completeness criteria.

The distribution of AMP across the year was tested against uniformly distributed random numbers. To do so, we generated 1 000 random uniform distributions of length  $N = 12$  and the resulting empirical distribution of the Gini coefficients was used to derive the 95% significance level from the resulting collection of estimates.

## 2.7. Diurnal distribution of AMP

We examined the diurnal distribution of  $AMP_{1-hr}$  by computing for each record the hourly frequency of  $AMP_{1-hr}$  as expressed by  $H_i (i = 1, \dots, n)$  with  $n = 24$  and by extracting the time of the day for the maximum number of occurrences (modal hour). We then compared the diurnal distribution of  $AMP_{1-hr}$  with that of the hourly peak intensity of  $AMP_{24-hr}$ . The Gini coefficient was also estimated for the diurnal distribution following the same method as described above.

## 2.8. Convection available potential energy conducive to $AMP_{1-hr}$ and $AMP_{24-hr}$

Atmospheric instability, often realized through the convection available potential energy (CAPE), is generally thought to facilitate the

occurrence of precipitation extremes. Indeed, CAPE is a widely used measure that reflects to some extent the vertical velocity, which controls the condensation rate and precipitation intensity (Lepore et al., 2015; Lenderink et al., 2017). CAPE may thus provide insight on how “convective” precipitation extremes are. We investigate here the dependency of both hourly and daily precipitation extremes on CAPE and how this dependency varies in different climatic regions. CAPE forecasts were extracted from ERA-Interim reanalyses (Dee et al., 2011) over the 1979–2016 period at 0.75° resolution. Forecasts are initialized at 0 000 and 1 200 UT and provide the instantaneous CAPE on a three-hourly basis. The three-hourly data has been interpolated to the GSDR gauges using a cubic weighting and then interpolated onto the hourly timescale using a spline function.

We examine CAPE both 24 h prior to and 24 h following  $AMP_{1-hr}$  and the hourly peak intensity of  $AMP_{24-hr}$  in the corresponding grid cell. We illustrate this relationship through four selected examples including Florida US, Kyushu Japan, northern Australia and the southern UK to elucidate how these events relate to atmospheric stability in both tropical and extra-tropical zones. We then examine for  $AMP_{1-hr}$  and  $AMP_{24-hr}$  the sensitivity to the maximum CAPE level observed over a period extending from 24 h prior to  $AMP_{1-hr}$  and to the hourly peak intensity of  $AMP_{24-hr}$  as CAPE is notoriously known to weaken as soon as precipitation forms. Stations are then pooled together based on the maximum CAPE levels associated to AMP following the procedure described in section 2.4. We report on the mean  $AMP_{1-hr}/AMP_{24-hr}$  as well as the distribution of recording sites along the CAPE gradient. Finally, we examine the sensitivity of  $AMP_{1-hr}$  ( $AMP_{24-hr}$ ) to both CAPE and storm duration (number of wet hours contributing to  $AMP_{24-hr}$ ) through a bivariate analysis.

### 3. Results and discussion

#### 3.1. Climatological features of $AMP_{1-hr}$ vs $AMP_{24-hr}$

Fig. 2 shows the 20-yr return levels of  $AMP_{1-hr}$  (Fig. 2a) and  $AMP_{24-hr}$  (Fig. 2b) along the AAP gradient. As expected,  $AMP_{24-hr}$  clearly intensify with AAP as seen in Benestad et al. (2012) with a rate of intensification close to 20%/500 mm year<sup>-1</sup> across a large moisture range. In other words, regions with higher AAP have also the highest daily extremes. Interestingly, this rate of intensification is somewhat lower for  $AMP_{1-hr}$  in regions with higher AAP and this result holds in both tropical and extra-tropical climates. This could be indicative of either an absence of relationship between hourly (convective) storms

and the moisture background in regions with higher AAP or a saturation effect of precipitation intensity. By contrast, the daily timescale aggregates light-to-moderate wet hours in precipitation-prone regions due to either favourable large-scale moisture advection or orographic effects collectively providing more scope for  $AMP_{24-hr}$  to increase at a higher rate. In other words, moisture availability and favourable circulation patterns are needed to sustain  $AMP_{24-hr}$  while this effect is more limited at the hourly timescale.

While both  $AMP_{1-hr}$  and  $AMP_{24-hr}$  are generally higher in the tropical zone, striking differences between  $AMP_{1-hr}$  and  $AMP_{24-hr}$  are evident in complex terrains (Fig. 3). Orographic enhancement of precipitation extremes featuring higher return levels along windward sides seem to emerge mostly in  $AMP_{24-hr}$  and are less pronounced in  $AMP_{1-hr}$  as seen along the west coast of the US, the eastern coastline of Australia (windward side of the Great Dividing Range) and peninsular Malaysia as well as the western coastlines of the UK (windward side of the Highlands) and India (windward side of the Western Ghats). This suggests that  $AMP_{1-hr}$  are mostly determined by the moisture content of storms and are, unlike their daily counterparts, less sensitive to orographic effects, corroborating the results reported in Fig. 2.

The concurrent intensity and  $\frac{AMP_{1-hr}}{P_{24-hr}} 100$  are highest in regions of low AAP (Fig. 4), exceeding 30% and 55% respectively at AAP below 1 500 mm year<sup>-1</sup>. The concurrent intensity exceeds 30% in India, parts of Australia and in the central US (Fig. 5), a region where both  $AMP_{1-hr}$  and  $AMP_{24-hr}$  are highly concentrated in spring/summer (see below section 3.2) due to the seasonal interaction of the Great Plain low-level jet with synoptic-scale flow (Wu and Raman, 1998). Collectively, these results suggest that hourly precipitation extremes in the central US are strong contributors to daily precipitation extremes. Also,  $\frac{AMP_{1-hr}}{P_{24-hr}} 100$  appears to be much lower along windward sides where large-scale and persistent systems can sustain long-duration storms and where orographic enhancement can sustain a near-constant distribution of high precipitation rates over 24-hr. This is particularly evident along the west coast of the US and the British Isles as well as the east coast of peninsular Malaysia and Japan.

The duration of storms initiating  $AMP_{1-hr}$  as well as the number of wet hours contributing to  $AMP_{24-hr}$  both increase with AAP (Fig. 6). Globally, we find that >70% (95%) of  $AMP_{1-hr}$  are embedded within 1–5 (1–10) hour storms (not shown) indicating that  $AMP_{1-hr}$  are associated on average with short-to-medium duration storms. This is particularly evident in the tropical zone (Fig. 6a), suggesting that the impact of cyclones on  $AMP_{1-hr}$  might be quite limited. Indeed, a tropical

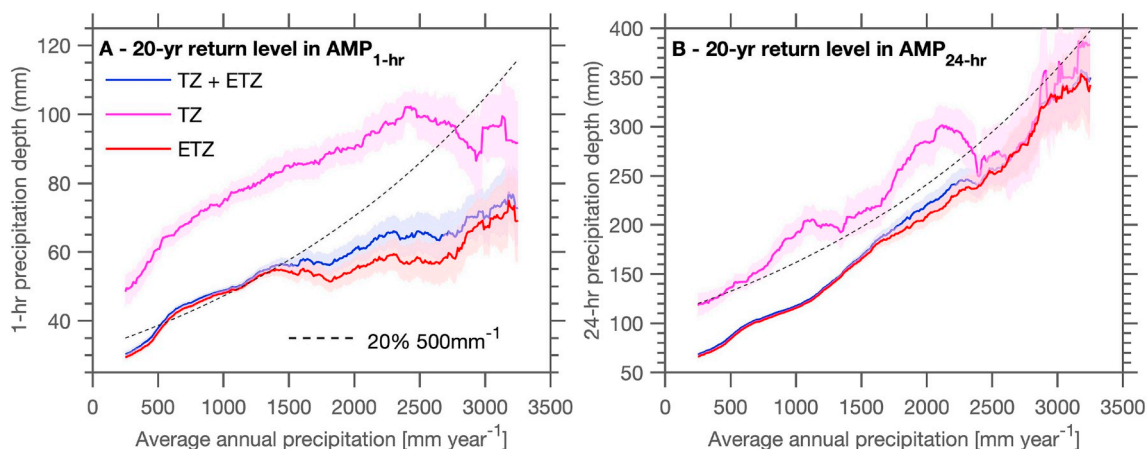


**Fig. 2.** 20-yr return level of a)  $AMP_{1-hr}$  and b)  $AMP_{24-hr}$  as a function of the climatological average annual precipitation (AAP) gradient in the tropical zone (TZ), extra-tropical zone (ETZ) and both tropical and extra-tropical zones combined (TZ + ETZ). The 20-yr return levels were estimated from a generalized extreme value distribution of AMP observed at each rain gauge. The 95% confidence intervals of the composite means were computed using 1 000 bootstrapped datasets sampling at random 50% of the records in each AAP bin. The envelope of confidence indicates the 2.5 and 97.5 percentile of the composite means from the bootstrapped datasets. The dashed lines indicate a rate of intensification of 20% 500 mm<sup>-1</sup>.

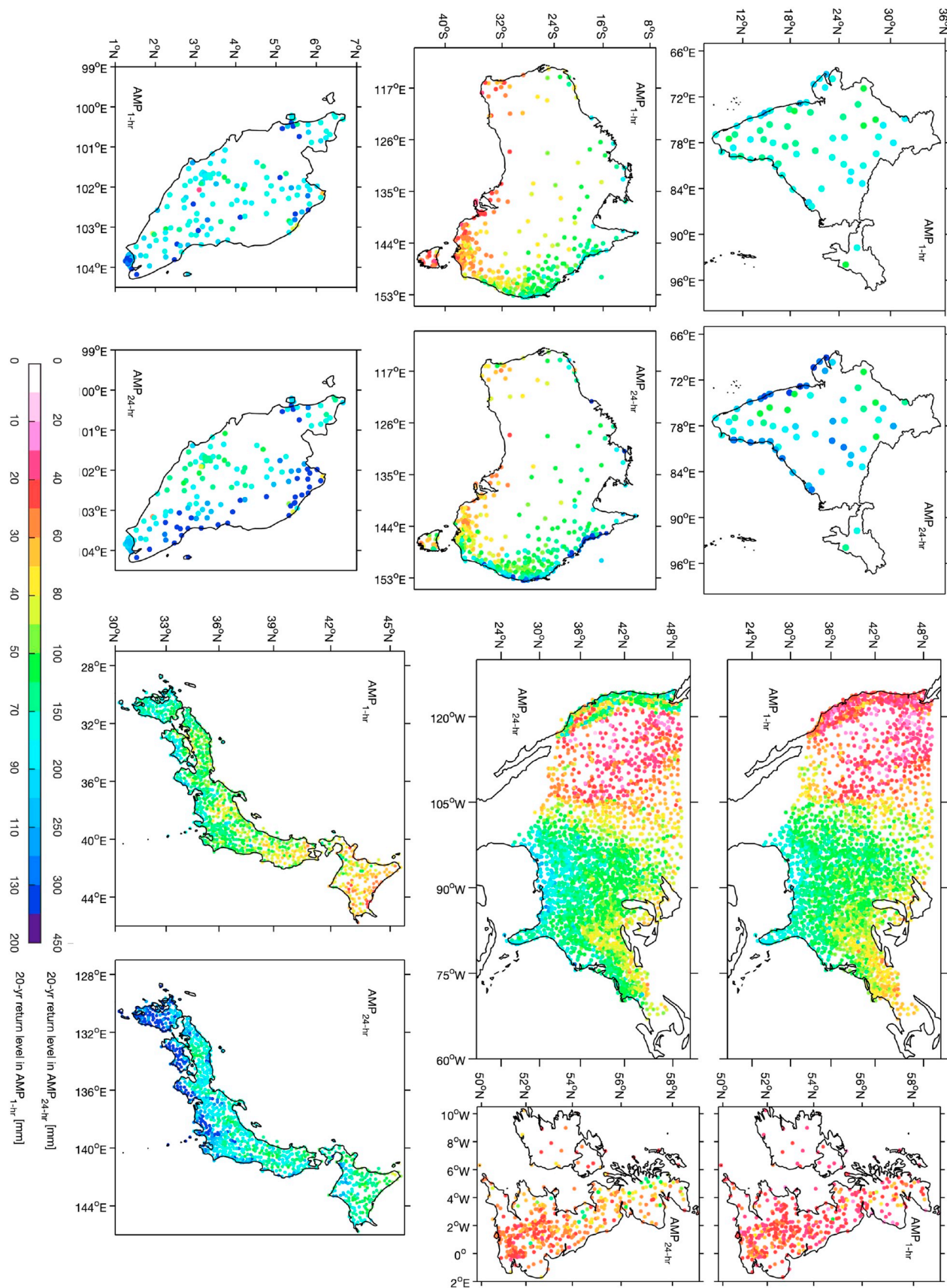


**Fig. 3.** 20-yr return level of  $AMP_{1-hr}$  and  $AMP_{24-hr}$ . The 20-yr return levels were estimated from a generalized extreme value distribution of AMP observed at each gauge. Note that the labels of the color bar indicate precipitation depth for  $AMP_{1-hr}$  (bottom) and  $AMP_{24-hr}$  (top). Both color bars are non-linear. (For interpretation of the references to color in this figure legend, the reader is referred to the Web version of this article.)



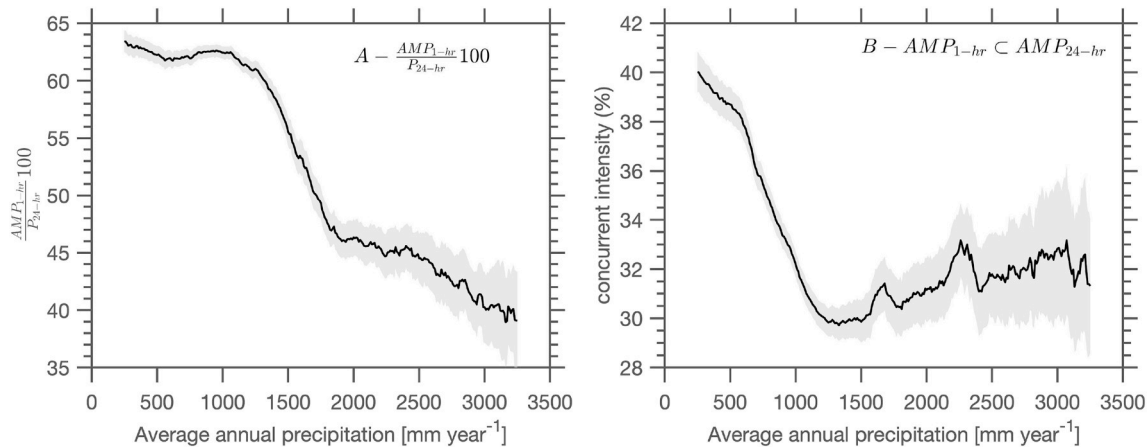


**Fig. 4.** a) Mean contribution (%) of  $AMP_{1-hr}$  to the corresponding total 1-day accumulation referred here to as  $\frac{AMP_{1-hr}}{P_{24-hr}} 100$  as a function of the average annual precipitation (AAP) gradient. b) Percent of  $AMP_{1-hr}$  embedded within  $AMP_{24-hr}$  with a 1-day tolerance referred to here as concurrent intensity as a function of the AAP gradient. The 95% confidence intervals of the composite means were computed using 1 000 bootstrapped datasets sampling at random 50% of the records in each AAP bin. The confidence envelope indicates the 2.5 and 97.5 percentile of the composite means from the bootstrapped datasets.

cyclone is unlikely to intercept landfall at the same location on an annual basis and the precipitation depth measured locally may not be as high as precipitation produced by a convective storm from the Eulerian perspective of a meteorological recording station. The primary exceptions are the US northwest coast and the coastal fringe of eastern Japan where storms initiating  $AMP_{1-hr}$  are much longer and may last a full day (Fig. 7).

More interesting is the limited number of wet hours contributing to  $AMP_{24-hr}$  (Fig. 6b). Globally, <10 (15) wet hours are responsible for >50% (80%) of  $AMP_{24-hr}$ . This can be seen across Australia (<10 wet hours), in the southeast of the British Isles (<10 wet hours), western Malaysia (<7 wet hours) or the central US (<5 wet hours) (Fig. 7) where precipitation extremes are often related to short-lived mesoscale convective complexes that have been found to persist for about 10 h (Laing and Fritsch, 1997). Using daily data in these regions would strongly underestimate the actual precipitation intensity during wet hours.

### 3.2. The seasonal distribution of $AMP_{1-hr}$ and $AMP_{24-hr}$

Two contrasting examples illustrating the seasonal timing as well as the degree of seasonality of both  $AMP_{1-hr}$  and  $AMP_{24-hr}$  are provided in Fig. 8. For a station located in Northeast, US (Fig. 8, a-b), it can be seen that the seasonality is stronger for  $AMP_{1-hr}$  (higher G) with a strong peak in July–August while  $AMP_{24-hr}$  are more spread throughout the year and can occur at other times of the year (lower G). This reflects the fact that intense hourly storms in this area are clearly locked onto the seasonal cycle of convection and occur only during summer months while longer-duration extremes, tied to large-scale circulation operating independently from the local convection, are more evenly spread throughout the year. However, a contrasting example in Malaysia (Fig. 8c–d) suggests that the seasonal distribution may become wider for shorter-duration AMP (lower G). Indeed, short-duration convective storms in this region are generally possible at any time of the year due to the proximity to ocean and overall high humidity levels with a preferential timing during the inter-monsoon seasons in peninsular Malaysia (Syafriana et al., 2015). Conversely, longer-duration extremes on the eastern side of the peninsula are strongly linked to seasonal large-scale monsoonal systems between December and March conveying enough moisture and favourable horizontal-vertical atmospheric structure to sustain precipitation extremes over daily or longer timescales. These two contrasting examples illustrate the complex seasonalities of precipitation extremes across timescales.

Fig. 9 focuses on the modal month of occurrence for  $AMP_{1-hr}$  and

$AMP_{24-hr}$  at each site and provides a more global picture of these seasonalities. While most  $AMP_{1-hr}$  and  $AMP_{24-hr}$  are well locked onto the seasonal cycle and clearly occur in the summertime across much of the eastern two-thirds of the US, Japan, the British Isles and across much of Australia and India, they can also take place in the winter across parts of the world including Northwest Scotland, the coastline of Southwest Australia or the west coast of the US when atmospheric rivers embedded within jet stream events penetrate inland and initiate extreme storms along the windward coast (Rutz et al., 2014; Barbero et al., 2018). The seasonality may change at a specific location across resolutions switching from a summer-driven regime for  $AMP_{1-hr}$  to a winter-driven regime for  $AMP_{24-hr}$  as seen in the Northeast US and the western windward side of the British Isles, reflecting the dominant role of large-scale (small-scale) systems in the cool (warm) season on longer-duration (shorter-duration) extremes. Changes in the seasonal timing of AMP over short distances may also reflect changes in wind regimes across the year, as seen in peninsular Malaysia where most  $AMP_{24-hr}$  along the eastern (western) side take place in December–January (late winter/early spring) during the Northeast (Southwest) Monsoon. Again, this windward/leeward contrast is less evident in  $AMP_{1-hr}$ , which are less dependent on large-scale circulation.

As expected, the seasonal concentration of  $AMP_{1-hr}$  is generally stronger (higher G) than that of  $AMP_{24-hr}$  (Fig. S2) but some opposing trends are found in India, along the east coast of Malaysia (Fig. 10) where  $AMP_{24-hr}$  occur specifically during the December–January monsoonal season (see Fig. 8, c-d) or along the coastal fringe of the western US where only cool-season atmospheric rivers can sustain such intensities over 24-hr (Lamjiri et al., 2017). The strongest seasonality for  $AMP_{1-hr}$  is observed in Japan, tropical northern Australia and in a region extending from New Mexico in the US to the northern Great Plains where precipitation is concentrated both seasonally and into intense storms (Canel and Katz, 2018). It is of interest to note that in these regions, the wet season is generally the season during which the AMP is most likely to occur. By contrast, the lowest seasonalities are mostly found in regions where AMP takes place outside the rainy season, as seen for instance in Malaysia or southern Australia. In other words, the seasonality of annual maxima tends to be greatest when AMP is cyclical (i.e. AMP takes place in the wet season), whereas it tends to be less when it is counter cyclical (i.e. AMP can occur in the dry season).

### 3.3. The diurnal distribution of $AMP_{1-hr}$ and the hourly peak intensity of $AMP_{24-hr}$

For each gauge we examine the modal hour of  $AMP_{1-hr}$  and of the



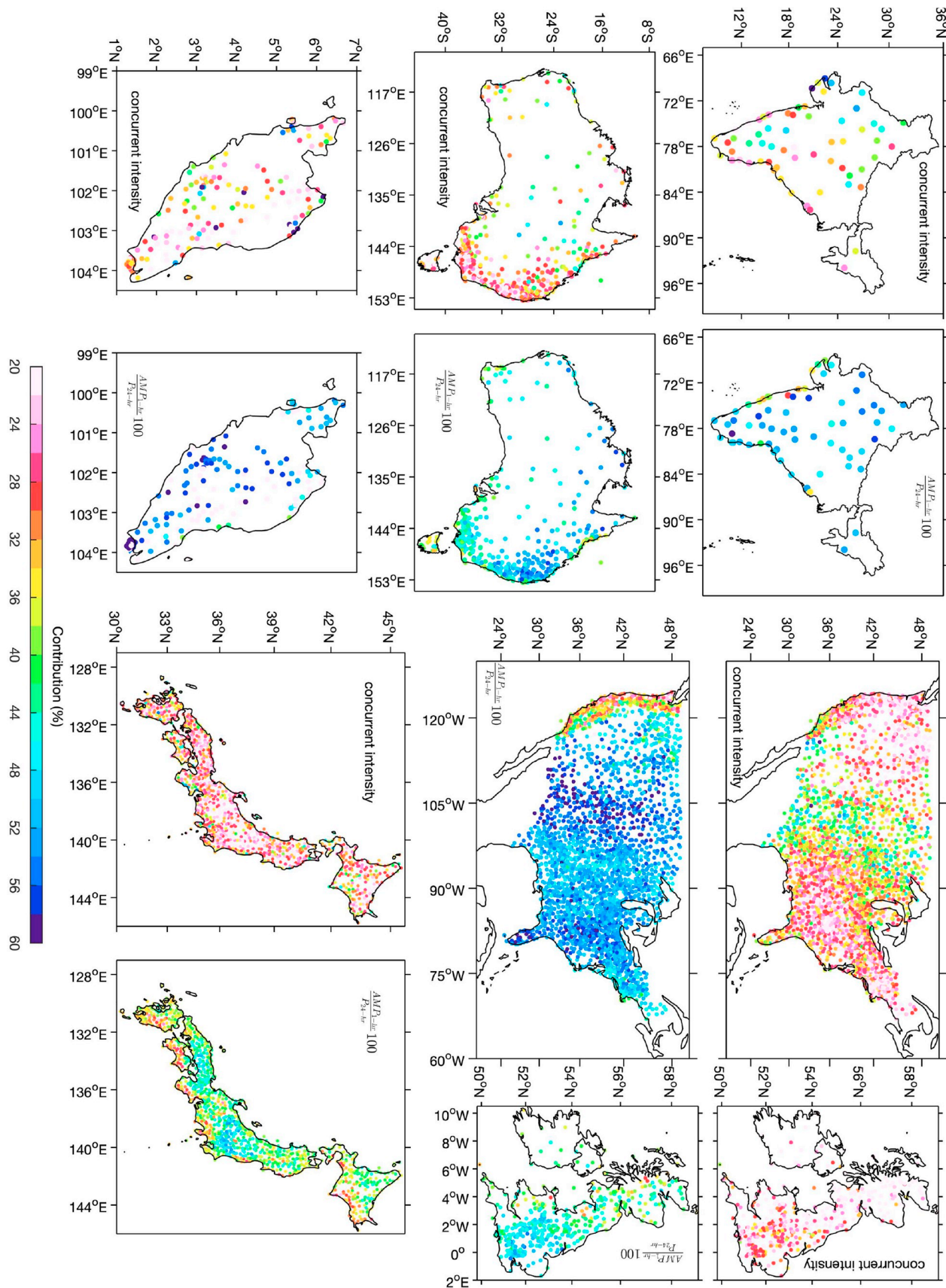


**Fig. 5.** Mean percent of  $AMP_{1-hr}$  embedded within  $AMP_{24-hr}$  with a 1-day tolerance (referred here to as concurrent intensity) and mean contribution (%) of  $AMP_{1-hr}$  to the corresponding total 1-day accumulation (referred here to as  $\frac{AMP_{1-hr}}{P_{24-hr}} 100$ ).

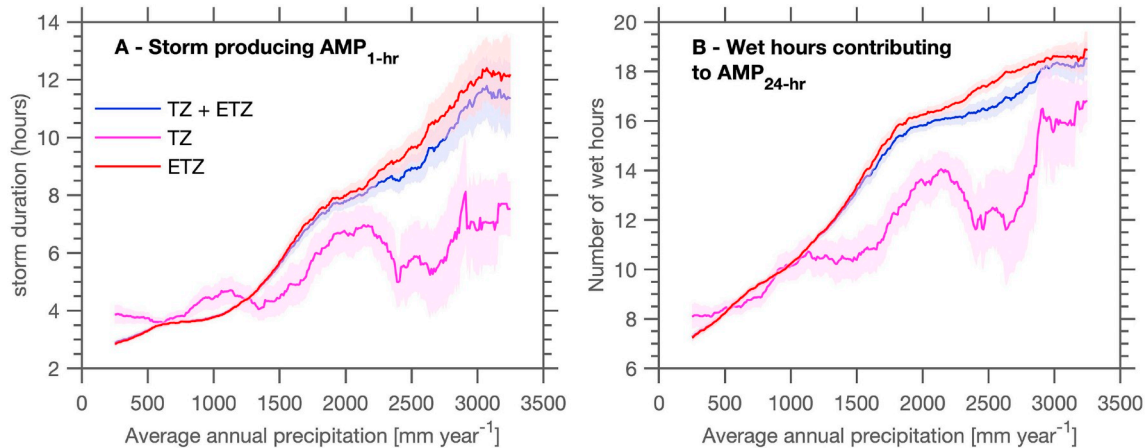


**Fig. 6.** a) Mean duration (hours) of storms initiating AMP<sub>1-hr</sub> as a function of the climatological average annual precipitation (AAP) gradient in the tropical zone (TZ), extra-tropical zone (ETZ) and both tropical and extra-tropical zones combined (TZ + ETZ). b) Same as a) but for the number of wet hours contributing to AMP<sub>24-hr</sub>. The 95% confidence intervals of the composite means were computed using 1 000 bootstrapped datasets sampling at random 50% of the records in each AAP bin. The confidence envelope indicates the 2.5 and 97.5 percentile of the composite means from the bootstrapped datasets.

hourly peak intensity of AMP<sub>24-hr</sub> (Fig. 11). The timing of these extremes involves a range of key mechanisms including the destabilization of the boundary layer due to thermal convection, topographic lifting or land-sea breezes (Evans and Westra, 2012). For a large portion of the regions, AMP<sub>1-hr</sub> occur preferentially in the late afternoon (from 17:00–20:00). Atmospheric instability through solar heating generally initiates moist convection in mid-afternoon, but convective systems reach their precipitation peak a few hours later. This is in agreement with previous analyses reporting on a similar peak in the mean hourly precipitation intensity in mid-to-late afternoon in summer over northern midlatitude land areas (Dai, 2001; Dai and Trenberth, 2004) and the tropical zone (Kikuchi and Wang, 2008). The diurnal distribution of AMP<sub>1-hr</sub> is clearly stronger (higher G) than that of the hourly peak intensity of AMP<sub>24-hr</sub> (which are more evenly distributed throughout the day) especially in Australia, Malaysia and Japan (see Fig. 11 but also Figs. S3 and S4), indicating that AMP<sub>1-hr</sub> is more dependent on the diurnal cycle. Surprisingly, AMP<sub>1-hr</sub> may also occur during the night (from 21:00–24:00) across large portions of the world including tropical Australia, Japan, India and the central part of Malaysia. This night-time peak had already been observed across the central US east of the Rockies (Ploshay and Lau, 2010; Mooney et al., 2017) due to the initiation and downslope propagation of moist convection over the Rockies and the adjacent Great Plains, but was generally thought to be an exception. The delay between the usual peak in the mean precipitation intensity in mid-to-late afternoon and the night-time occurrence of AMP<sub>1-hr</sub> in many regions may relate to the size and the organization of the systems initiating AMP<sub>1-hr</sub>. It is likely that these annual maxima are related to large convective systems. Precipitation-cell size and intensity have been shown to be positively correlated (Lochbihler et al., 2017). Indeed, large organized mesoscale convective systems have lifetimes often exceeding 6–10 h (Feng et al., 2012) and often reach their maximum extent during nighttime (Laing and Fritsch, 1997), which could be related to radiation effects or the occurrence of a nocturnal low-level jet feeding intense convection (Laing and Fritsch, 1997), but also to the time needed to amalgamate smaller cloud systems into larger organized structures (Houze Jr, 2004; Moseley et al., 2016).

AMP<sub>1-hr</sub> also take place later (from 21:00–24:00) in the central part of Malaysia and a few hours earlier (from 17:00–20:00) in the northern and southern parts of the peninsular. This may be due to the combination of moisture flux convergence with the longitudinal extent of the peninsular expanding in the central part and thus delaying the timing of AMP<sub>1-hr</sub> with respect to coastal regions further south and north. This propagation of the diurnal cycle with AMP<sub>1-hr</sub> occurring earlier in coastal regions and propagating inland is also evident to some extent in

other islands such as Japan and the British Isles and is often referred to as the diurnal marches (Garreaud and Wallace, 1997).

Early morning timings in the hourly peak intensity of AMP<sub>24-hr</sub> around 05:00–08:00 are evident across parts of the US but also in coastal sectors of Japan, Southern Australia or the western side of the British Isles as seen in Covey et al. (2016) and Kikuchi and Wang (2008) due to a peak in relative humidity (Dai, 2001) and to the differential heating between water and land surfaces that can generate local circulations. Very few AMP<sub>1-hr</sub> occur at that time of the day in our analysis suggesting that this early timing pertains only to less intense long-duration storms as recently observed in the UK (Xiao et al., 2018).

#### 3.4. Atmospheric stability associated to AMP<sub>1-hr</sub> and AMP<sub>24-hr</sub>

Fig. 12 illustrates the actual CAPE level observed 24 h prior to and 24 h after AMP<sub>1-hr</sub> and the hourly peak intensity of AMP<sub>24-hr</sub> in four selected regions of the world spanning tropical (Northern Australia), subtropical (Kyushu, Southern Japan and Florida, Southeast US) and midlatitude (Southern part of the British Isles) climates. AMP<sub>1-hr</sub> are clearly associated with higher CAPE compared to the hourly peak intensity of AMP<sub>24-hr</sub> and, in both cases, CAPE reaches a maximum 1–2 h before the peak intensity of precipitation. The slight delay between the peak in CAPE and AMP<sub>1-hr</sub> is not surprising as deep convection is expected to weaken CAPE through different mechanisms, including the upward transfer of heat released by the condensation of latent heat and the downdrafts cooling the lower troposphere through evaporation (Davies et al., 2013; Dong et al., 2018). Previous studies have suggested that antecedent CAPE might be a better predictor for subsequent convective precipitation (Davies et al., 2013). The secondary peak seen in Florida likely reflects the lag between the timing of some AMP with respect to the strong diurnal cycle included in CAPE in this region.

Based on the whole dataset, Fig. 13 shows that AMP<sub>1-hr</sub> (AMP<sub>24-hr</sub>) intensify with increasing CAPE until 1 500 (1 000) Joules kg<sup>-1</sup>, a threshold above which AMP<sub>1-hr</sub> (AMP<sub>24-hr</sub>) saturates as observed in regional analyses in China (Dong et al., 2018), the central US (McCorkle et al., 2016) and northern Australia (Davies et al., 2013). This saturation effect in precipitation intensity in response to CAPE shows that additional factors such as specific humidity or dew point temperature (Lepore et al., 2015) also play a role at higher CAPE levels. As expected, this saturation effect emerges in AMP<sub>24-hr</sub> first as high CAPE is in general very localized and favours rather short-lived intense storms. Long-lasting precipitation systems such as tropical cyclones, mesoscale convective complexes or frontal systems have in general low-to-moderate CAPE levels but cover large areas and move relatively

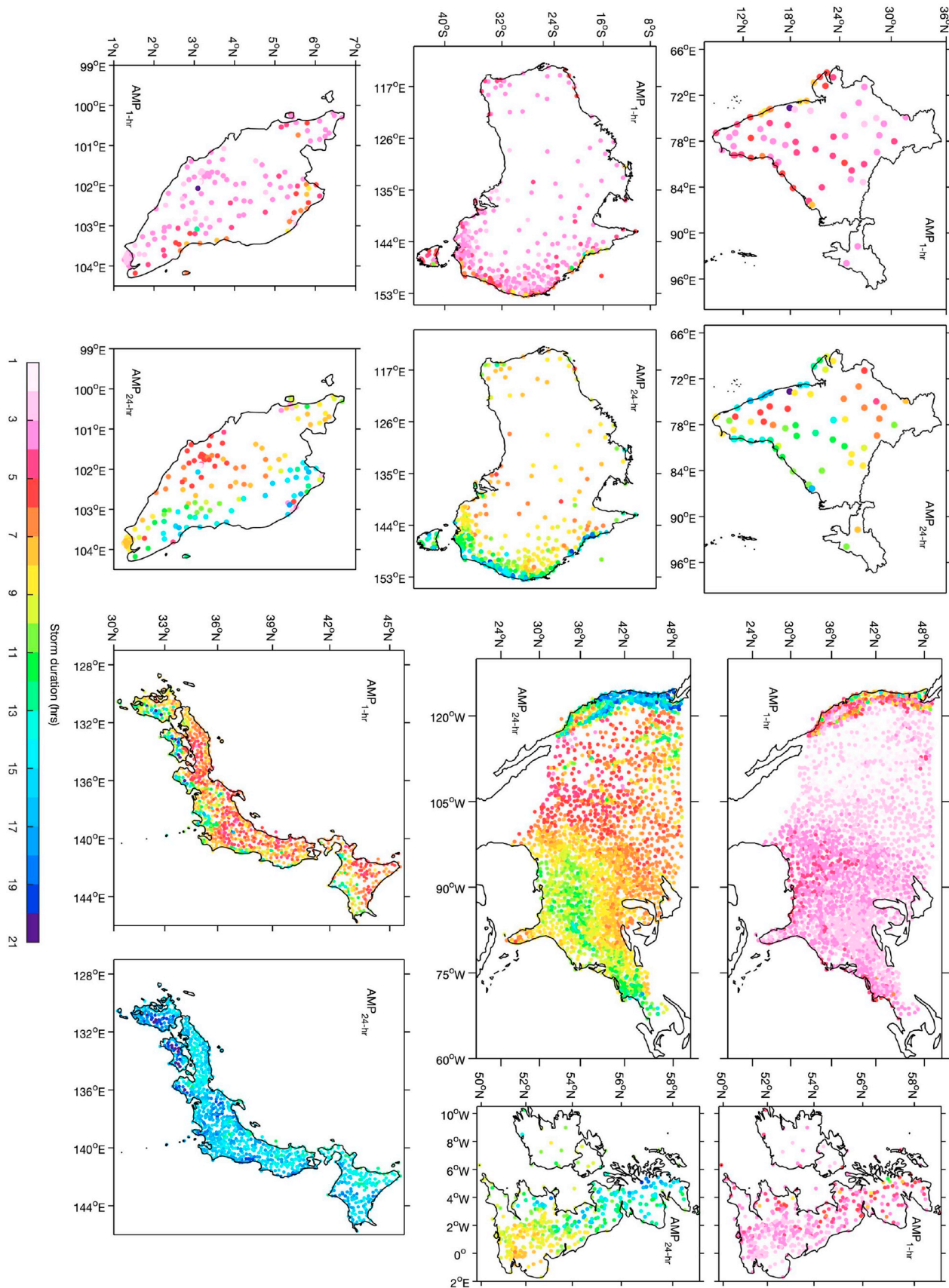


**Fig. 7.** Mean duration (hours) of storms initiating AMP<sub>1-hr</sub> and number of wet hours contributing to AMP<sub>24-hr</sub>.



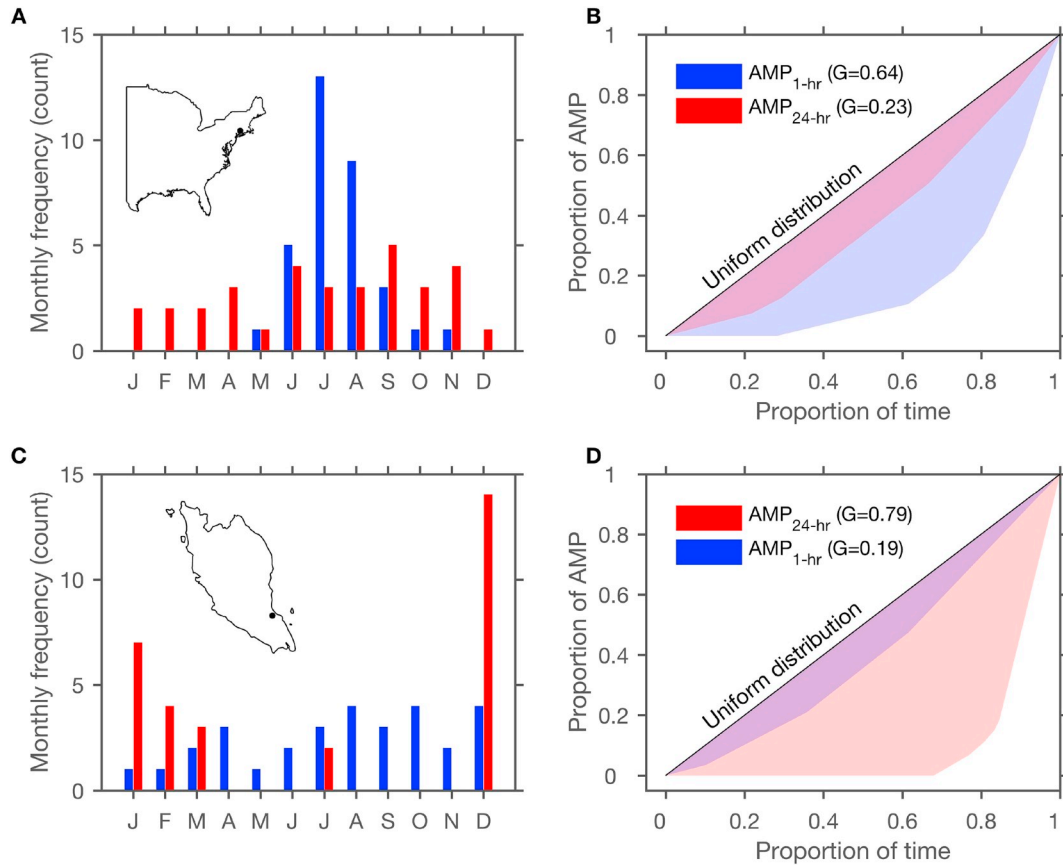


**Fig. 8.** a) Example of the monthly distribution of AMP<sub>1-hr</sub> (blue) and AMP<sub>24-hr</sub> (red) for one station in the Northeast US. b) The Gini coefficient is reported for each resolution and is calculated as twice the area between the 1:1 line and the Lorenz curve representing the relationship between the proportion of time and the proportion of AMP (see Methods for further details). c-d) Same as a-b but for one station in Malaysia. (For interpretation of the references to color in this figure legend, the reader is referred to the Web version of this article.)

slowly, resulting locally in large precipitation accumulations contributing to AMP<sub>24-hr</sub>.

By contrast, the relation between CAPE and AMP<sub>1-hr</sub> is stronger in both tropical and extra-tropical zones as elevated CAPE levels over land have been linked to scattered thunderstorms (Rutledge et al., 2002) whose limited spatial extent do not really inhibit the surface warming and the resulting CAPE. However, a saturation effect in AMP<sub>1-hr</sub> is still observed at  $1500 \text{ J kg}^{-1}$  (although this threshold is likely to vary regionally) and is likely due to the short life cycle of convective storms (<1 h) at higher CAPE levels. Dong et al. (2018) and Lepore et al. (2015) also noted that the conversion of CAPE into kinetic energy becomes less efficient at higher CAPE and that convective inhibition may suppress the occurrence of updrafts even in the presence of higher CAPE levels. Additionally, higher CAPE levels with vertical wind shear and a strong steering flow can both contribute to fast-moving deep convective systems, producing low local precipitation amounts.

Higher CAPE levels coincident with or prior to AMP<sub>1-hr</sub> are seen in the central US and central Japan (Fig. 14), suggesting that the late-afternoon and night-time AMP<sub>1-hr</sub> in these regions (Fig. 11) are mostly convective in nature. While AMP<sub>1-hr</sub> are associated with average maximum CAPE levels ranging from  $1000$  to  $1500 \text{ J kg}^{-1}$  across peninsular Malaysia, AMP<sub>24-hr</sub>, generally thought to relate to large-scale monsoonal systems, take place under more stable conditions along the windward side, with CAPE values ranging from  $300$  to  $800 \text{ J kg}^{-1}$ , highlighting the weaker influence of convective processes on daily extremes. These CAPE levels are above average for the time of the year (Fig. S5), especially during AMP<sub>1-hr</sub> events, suggesting that the difference between CAPE-triggering AMP<sub>1-hr</sub> and AMP<sub>24-hr</sub> is not only due to their seasonality.

Finally, Fig. 15 summarizes some of the results shown above by depicting the overall mean AMP<sub>1-hr</sub> across all regions in a two-dimensional space depicted by both CAPE level and the duration of storm producing AMP<sub>1-hr</sub>. As shown previously, AMP<sub>1-hr</sub> are more sensitive to the spatial CAPE gradient (Fig. 15, left) and less sensitive to storm duration (Fig. 15, top). Note that AMP<sub>1-hr</sub> increases with storms >15 h but these conditions are only representative of a few sites mostly located in southern Japan (see Fig. 7). The climate-niche associated with the highest mean AMP<sub>1-hr</sub> was defined by a CAPE level ranging from  $1300$  to  $1600 \text{ J kg}^{-1}$  (Fig. 15, middle) and storm duration ranging from  $10$  to  $15$  h storms. By contrast, mean AMP<sub>24-hr</sub> clearly increases in a linear fashion with an increasing number of wet hours (Fig. 16, top) but responds only modestly to increased CAPE (Fig. 16, left) with most AMP<sub>24-hr</sub> fed by  $10$ – $15$  wet hours under rather low CAPE conditions. This recipe is obviously likely to vary regionally.

#### 4. Summary

This study provides 1) a multi-continental climatology of observed hourly and daily precipitation extremes, their magnitude, and their dependence on climatological average annual precipitation (AAP), 2) the mean length of storm producing hourly precipitation extremes as well as the mean number of wet hours responsible for daily extremes, 3) a climatology of their seasonal distribution, 4) a climatology of their diurnal distribution, and 5) an assessment of their dependence on atmospheric stability across different climatic regions. The primary conclusions are:



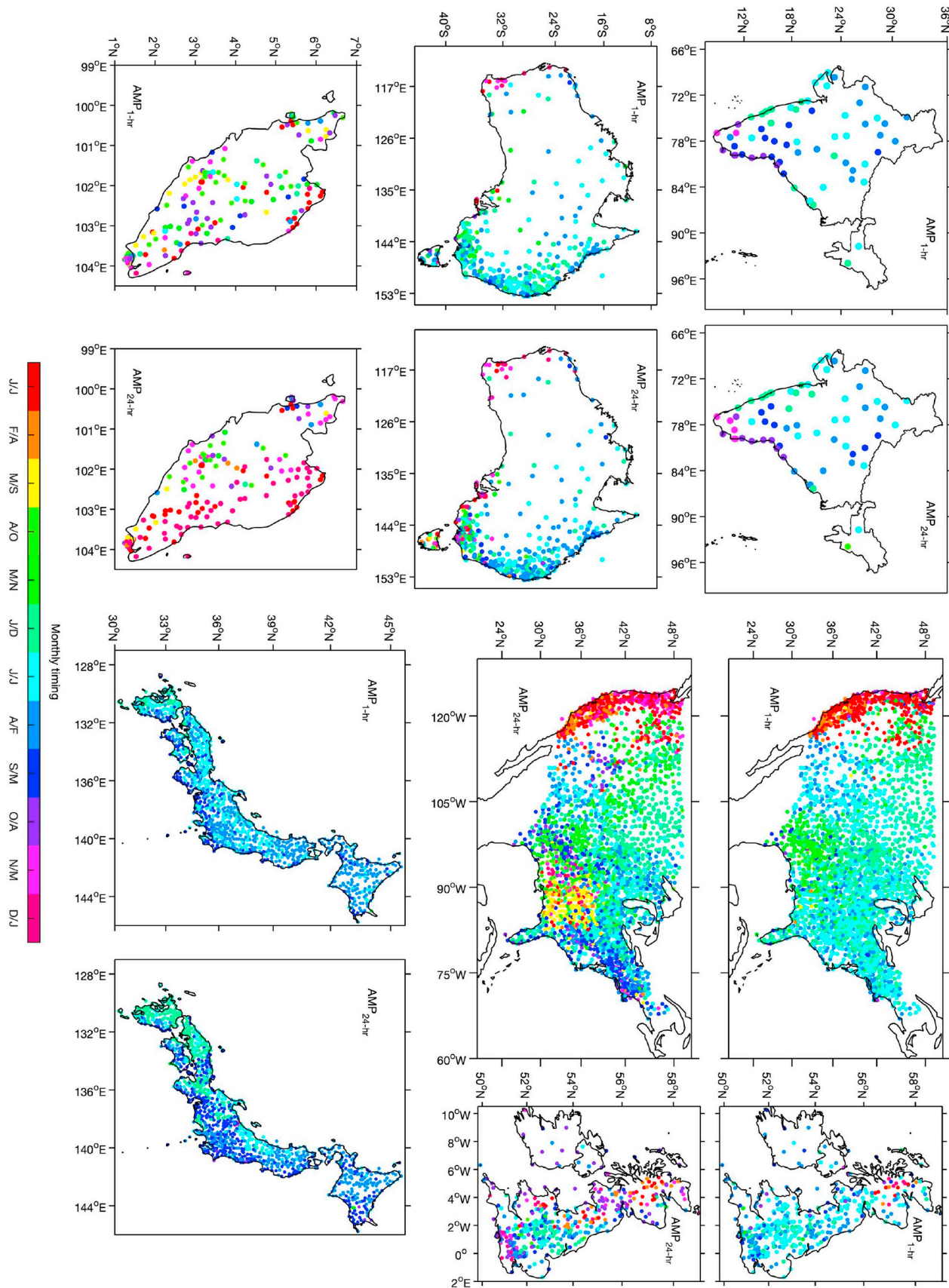


**Fig. 9.** Modal month of occurrence for AMP<sub>1-hr</sub> and AMP<sub>24-hr</sub>. The seasonality was reversed for the southern hemisphere such that the colorbar refers to the same climatological month in both hemispheres. For example, J/J refers to January/July for the northern and southern hemisphere, respectively.

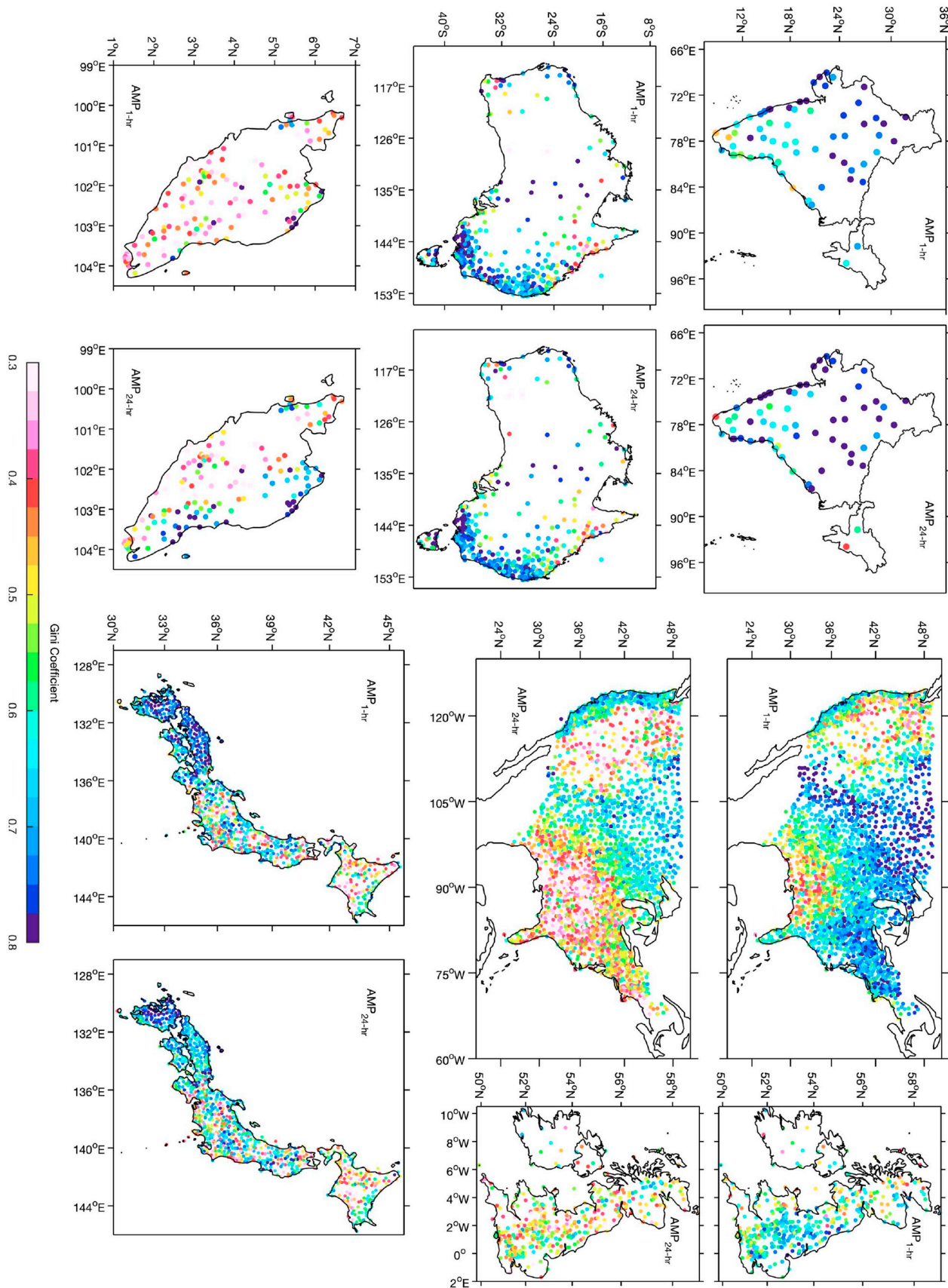


**Fig. 10.** Monthly distribution of AMP<sub>1-hr</sub> and AMP<sub>24-hr</sub> as measured by the Gini coefficient. Gini coefficients exceeding 0.46 are statistically significant at the 95% confidence level. The significance was estimated from 1 000 random uniform distributions of length  $N = 12$ . The resulting empirical distribution was then used to derive the 95% significance level from the resulting collection of estimates.



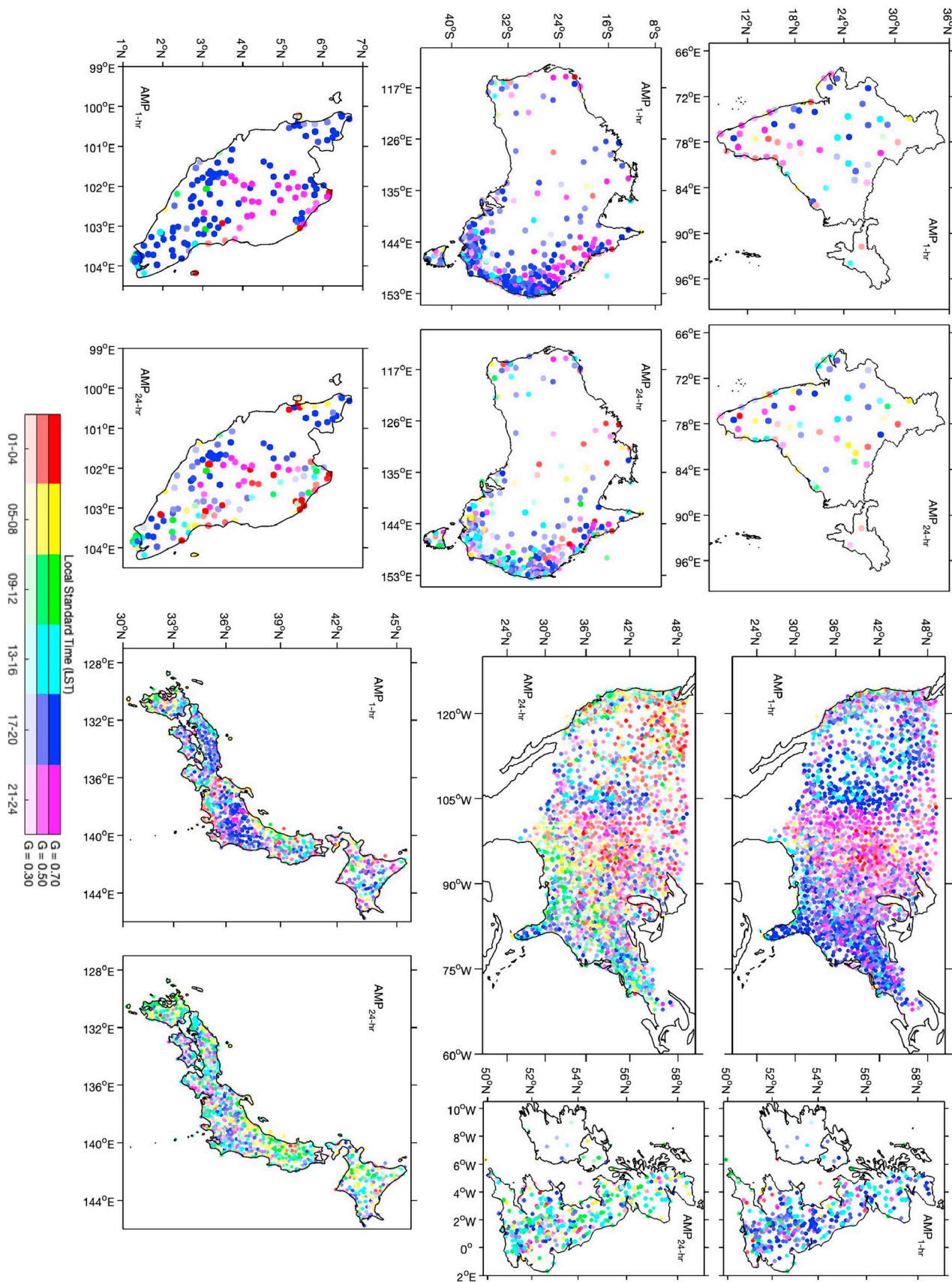


**Fig. 11.** Modal 4-h blocks during which AMP<sub>1-hr</sub> and the hourly peak intensity of AMP<sub>24-hr</sub> take place. Following [Evans and Westra \(2012\)](#), the saturation/-transparency indicates the strength of the diurnal distribution as measured by the Gini coefficient. Gini coefficients exceeding 0.42 are statistically significant at the 95% confidence level. The significance was estimated from 1 000 random uniform distributions of length  $N = 24$ . The resulting empirical distribution was then used to derive the 95% significance level from the resulting collection of estimates.

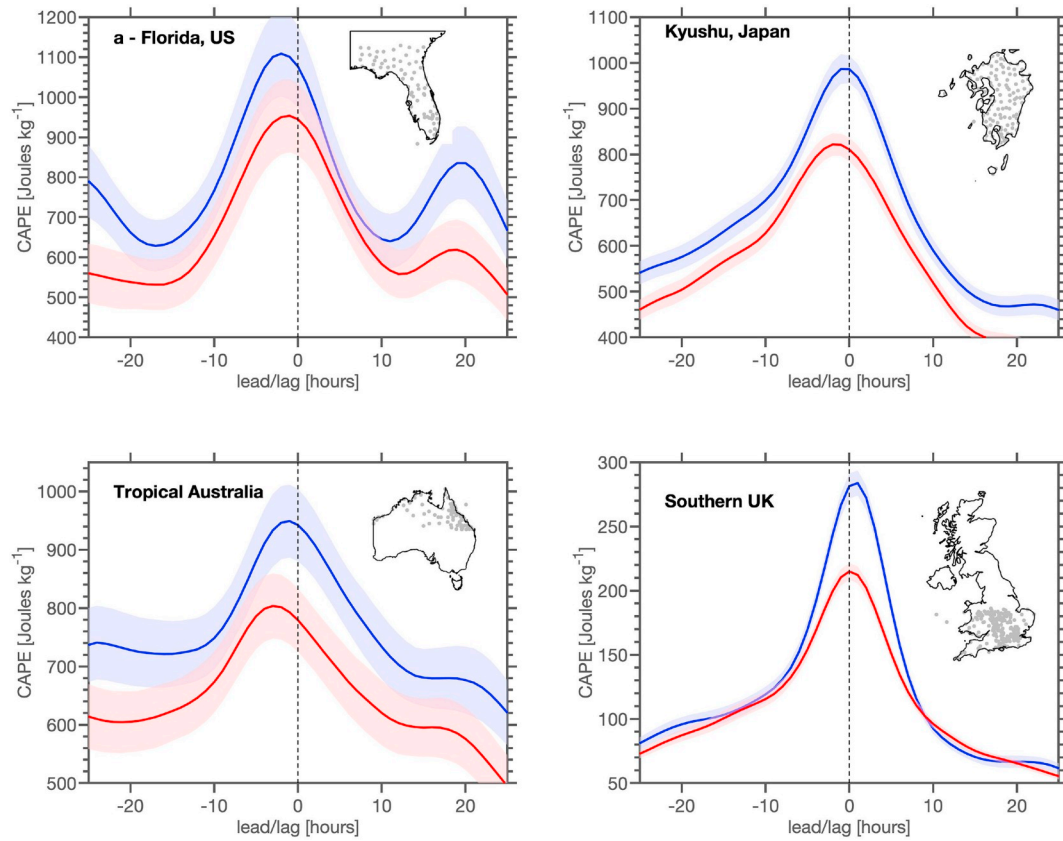


**Fig. 12.** Actual CAPE both 24 h prior to and 24 h following  $AMP_{1-hr}$  (blue) and the hourly peak intensity of  $AMP_{24-hr}$  (red) in four specific regions. The 95% confidence intervals of the composite means were computed using 1 000 bootstrapped datasets sampling at random 50% of the records in each region (see map in the insert). The confidence envelope indicates the 2.5 and 97.5 percentile of the composite means from the bootstrapped datasets. (For interpretation of the references to color in this figure legend, the reader is referred to the Web version of this article.)

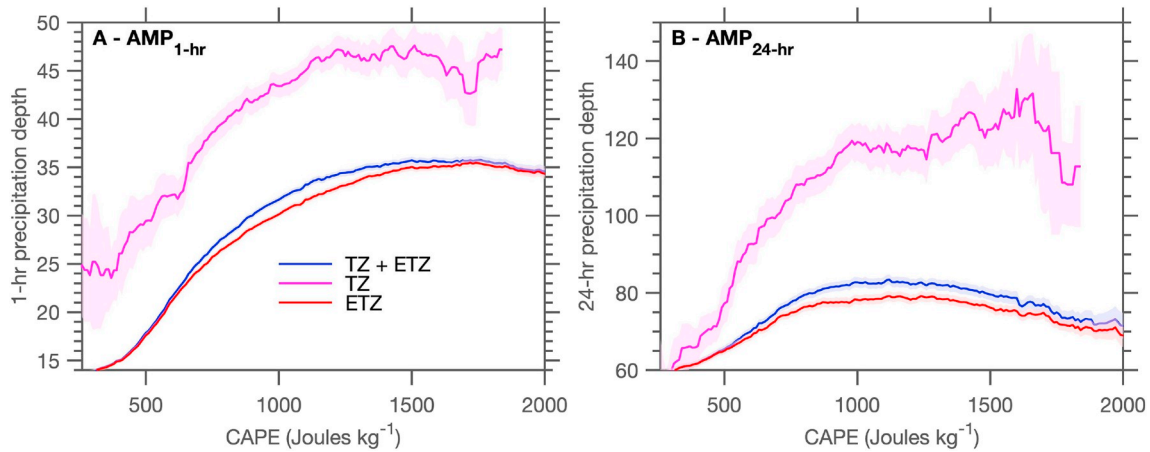


**Fig. 13.** a) Mean  $AMP_{1-hr}$  and b)  $AMP_{24-hr}$  as a function of the maximum CAPE level observed over a period extending from 24 h prior to  $AMP_{1-hr}$  and to the hourly peak intensity of  $AMP_{24-hr}$  in the tropical zone (TZ), extra-tropical zone (ETZ) and both tropical and extra-tropical zones combined (TZ + ETZ). The 95% confidence intervals of the composite means were computed using 1 000 bootstrapped datasets sampling at random 50% of the records. The confidence envelope indicates the 2.5 and 97.5 percentile of the composite means from the bootstrapped datasets.

1) The magnitude of AMP correlates to the APP, with a rate of intensification of the 20-year return level of  $AMP_{24-hr}$  of about 20% per  $500 \text{ mm year}^{-1}$  increase in the AAP. We find that  $AMP_{1-hr}$  intensify at a slower rate but this does not prove that there is an upper constraint on short-duration extremes or a theoretical maximum of how intense  $AMP_{1-hr}$  can be. Hourly data mostly reflects the convective scale which is thought to be relatively constant across different climates, as opposed to daily data that integrates

convection but also other processes responsible for precipitation duration such as large-scale dynamics, orographic effects, the spatial extent of the storm and its travelling speed. The link between wet-day mean precipitation and daily precipitation extremes has already been emphasized by Benestad et al. (2012) and may be used to deduce information on extreme values from the climatological state of a given site. Similar methods linking the AAP, the wet-hour mean precipitation or another metric based on the entire distribution



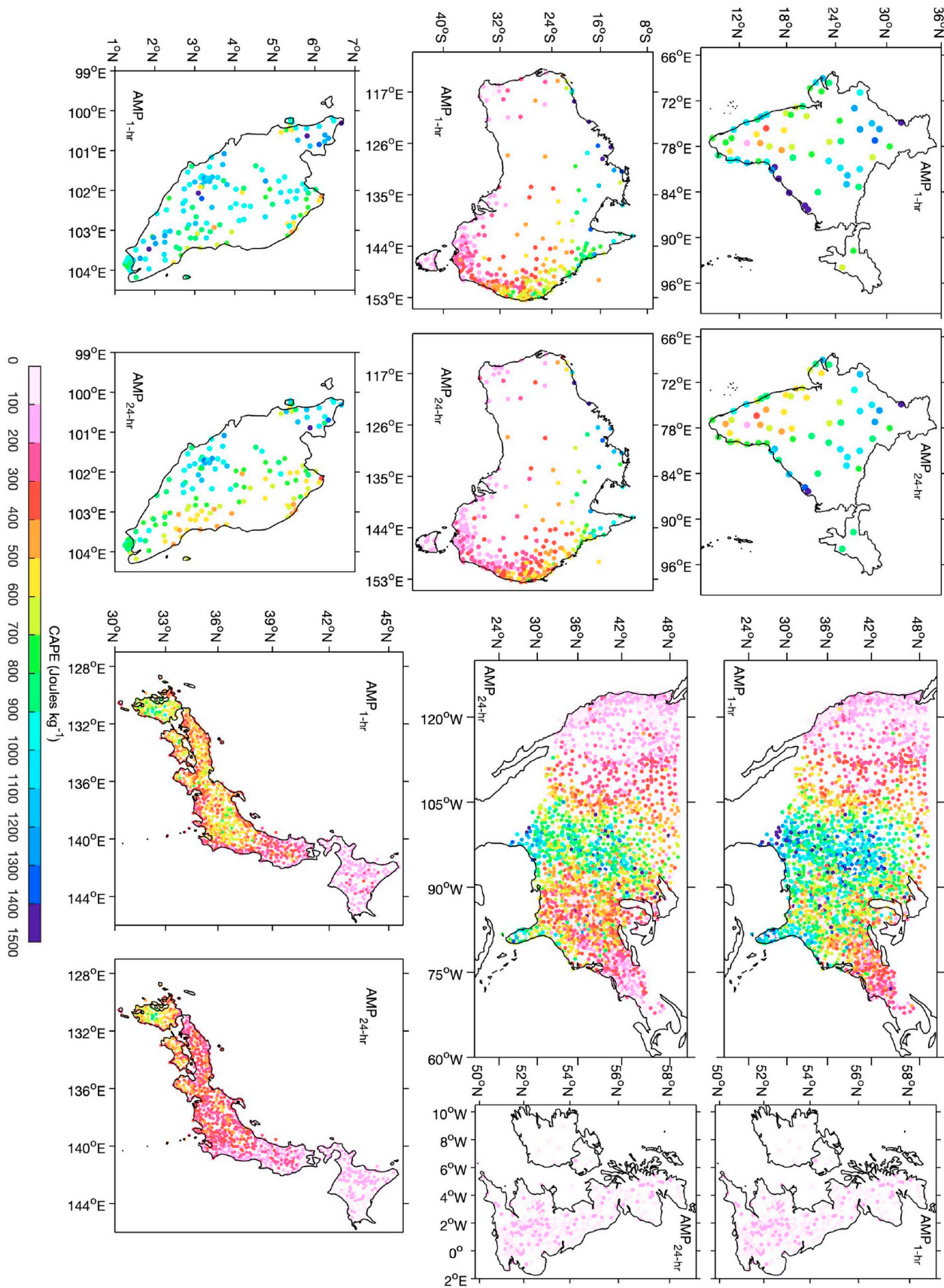
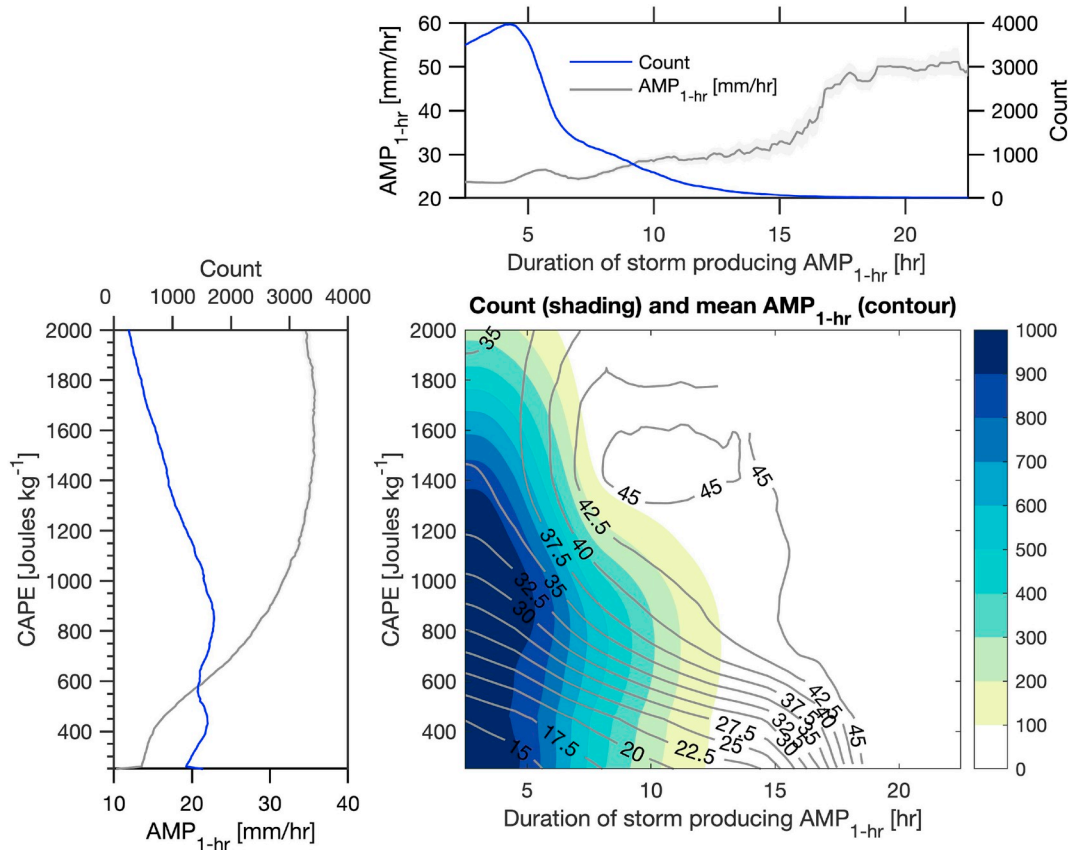


Fig. 14. Average maximum CAPE level observed over a period extending from 24 h prior to AMP<sub>1-hr</sub> and to the hourly peak intensity of AMP<sub>24-hr</sub>.



**Fig. 15.** Left) Mean  $AMP_{1-hr}$  (gray, bottom axis) and count of recording sites (blue, top axis) as a function of the maximum CAPE level observed over a period extending from 24 h prior to  $AMP_{1-hr}$ . Top) Mean  $AMP_{1-hr}$  (gray, left axis) and count of recording sites (blue, right axis) as a function of the mean duration (hours) of storms initiating  $AMP_{1-hr}$ . Middle) Bivariate analysis of the influence of CAPE (left axis) and the duration of storms initiating  $AMP_{1-hr}$  (bottom axis) on mean  $AMP_{1-hr}$  (contour) and on the distribution of recording sites (shading). (For interpretation of the references to color in this figure legend, the reader is referred to the Web version of this article.)

of hourly rainfall to extreme events would be valuable when sample size issues arise.

- 2) Most  $AMP_{1-hr}$  are initiated by short-duration storms (1–5 h), with storm duration increasing with AAP. Likewise,  $AMP_{24-hr}$  are found to be the product of a limited number of wet hours ranging from about 7 h in regions of low AAP to 18 h in regions of high AAP, highlighting the added-value of hourly data in estimating actual precipitation intensity.
- 3) The seasonal distribution of AMP varies across different timescales and reveals complex patterns, with regional variations reflecting the prevalence of different seasonal triggering mechanisms. Most  $AMP_{1-hr}$  in the midlatitudes are found to be strongly locked onto the seasonal cycle and generally occur during summer-time while  $AMP_{24-hr}$  occur more evenly throughout the year. The seasonality of AMP can even switch at a specific location across different durations. This general pattern may reverse in monsoonal climates where the seasonality of  $AMP_{24-hr}$  is better defined than that of shorter-duration AMP due to their strong dependence on the seasonal migration of large-scale systems such as the inter-tropical convergence zone.
- 4)  $AMP_{1-hr}$  occur preferentially in late afternoon to late evening in most parts of the world, slightly later than the peak generally observed in the mean diurnal cycle of precipitation intensity. This delay may be due to the fact that the most intense storms accumulate energy and moisture over a longer period and then produce more intense precipitation once released. Alternatively,  $AMP_{1-hr}$  may originate from organized convection that needs more time to develop than single cell convective storms. In other words, the longer the

moisture building content, the more intense the storm. As  $AMP_{1-hr}$  occur by definition once a year, they are not expected to contribute substantially to the diurnal distribution of the mean hourly precipitation intensity.

- 5)  $AMP_{1-hr}$  are correlated to a certain extent to CAPE, confirming the prevalence of convective processes in shorter-duration precipitation extremes. However, the response of precipitation intensity is not linear and levels off beyond a certain CAPE threshold. This result is however not unexpected given that precipitation intensity is a function of both CAPE and the amount of moisture available (Lepore et al., 2015, 2016; Dong et al., 2018). The CAPE-precipitation intensity relationship saturates even more quickly for  $AMP_{24-hr}$ , for which atmospheric instability plays only a secondary role.

These results have multiple implications. As reported in previous works, the intermittent nature of precipitation is masked out in daily data, especially in the less precipitation-prone regions. For instance (Pendergrass and Knutti (2018)), have recently shown that half of total annual precipitation falls in only a few days across many regions of the world. This unevenness is expected to be stronger in hourly data given that precipitation is intermittent from one day to another but also within a day. Sub-daily data also enables a better characterization of the true precipitation intensity as well as a better understanding of processes driving extremes. Given the growing interest in sub-daily precipitation extremes in the literature, the hourly precipitation dataset used here can provide the hydroclimate community with better information on intensities initiating flash floods.

It is of interest to note that the seasonality of daily precipitation

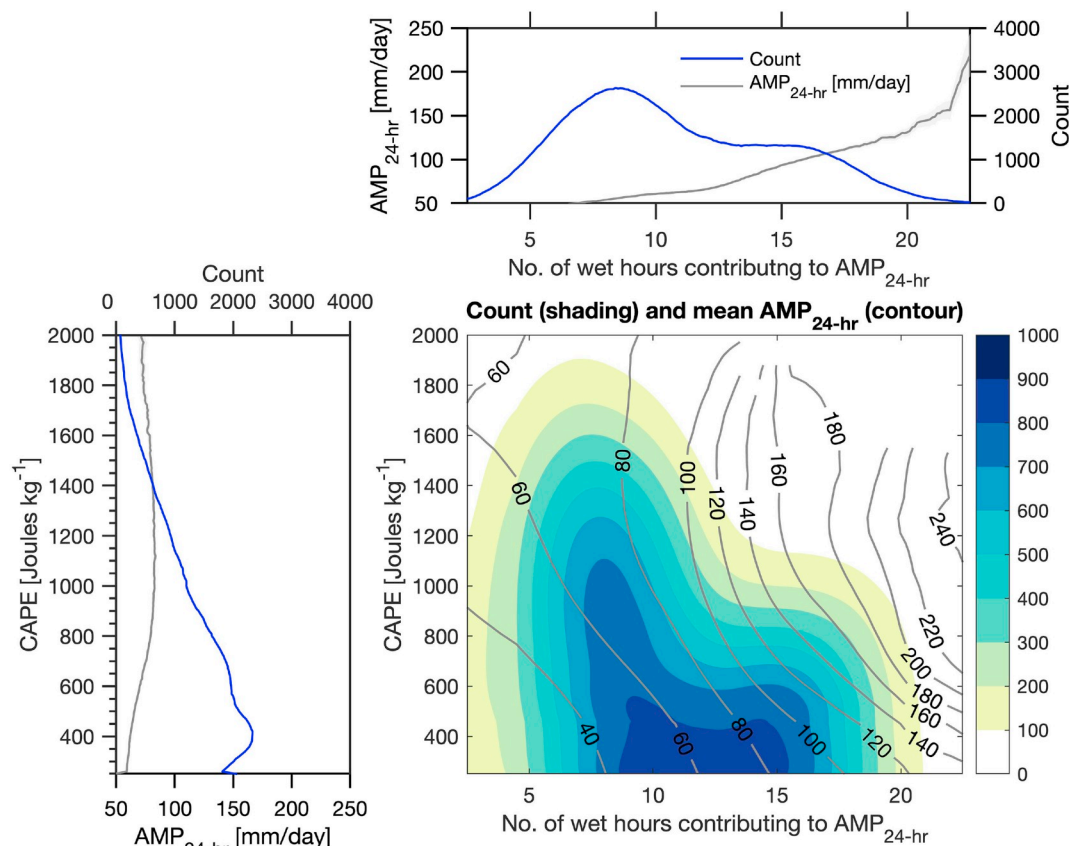


Fig. 16. Same as figure 15 but for  $AMP_{24-hr}$ .

extremes shown here contrasts somewhat with the seasonality of daily flooding depicted in previous studies (Villarini, 2016), highlighting the dominant role of antecedent conditions in triggering floods (Berghuijs et al., 2016; Bennett et al., 2018). A comparison of short-duration precipitation and flash-flood seasonality may also help to better elucidate different triggering mechanisms for regional flash flooding.

Results reported here may also be useful for climate model evaluation. For instance, the ability of models to reproduce the storm duration initiating the annual maxima or other features such as the switch in the seasonality of extremes across durations at a specific site could be evaluated. In this regard, the use of the Gini coefficient might be useful in model evaluations as it summarizes the temporal distribution of precipitation through a day or a year into one single value. The late-afternoon and night-time peak in the most extreme hourly extremes should be evaluated in climate models as well. This is of primary importance as most models generally fail to simulate the diurnal cycle of precipitation in regions where the phase of the observed cycle of precipitation does not coincide with the time of maximum surface temperature (Mooney et al., 2017) although convection permitting models (CPMs) have been found to simulate the diurnal cycle more realistically (Kendon et al., 2012; Prein et al., 2015).

The main limitation of this study is the uneven distribution of rain gauges across space. All statistics are based on hourly data-covered regions and thus only reflect the sampled regions. A quality control process of the GSDR dataset is currently underway in other regions and will soon provide a more complete coverage that could be used to more accurately quantify sub-daily precipitation features on a more global scale.

Finally, further studies are needed to detect the effects of global warming on short-duration precipitation extremes across the world. Global trend detection studies have so far relied on daily data (Westra et al., 2013; Donat et al., 2017; Sippel et al., 2017) but the aggregation of

precipitation across a day may affect the sign of the trend in extreme precipitation (Zheng et al., 2015; Morbidelli et al., 2018). A recent study suggests that changes in hourly extremes may emerge before daily extremes (Kendon et al., 2018). On the other hand, trends in sub-daily extremes have only been examined in nation-wide studies (Barbero et al., 2017; Guerreiro et al., 2018; Ali and Mishra, 2018) and a more global assessment is still lacking. The GSDR dataset provides for the first time the opportunity to examine these research questions across different climate zones with a consistent methodology and assess some of the World Climate Research Programme (WCRP) Grand Challenges on Weather and Climate Extremes.

## Acknowledgments

This work was supported by the INTENSE project. INTENSE is supported by the European Research Council (grant ERC-2013-CoG-617329). Hayley Fowler is funded by the Wolfson Foundation and the Royal Society as a Royal Society Wolfson Research Merit Award holder (grant WM140025).

## Appendix A. Supplementary data

Supplementary data to this article can be found online at <https://doi.org/10.1016/j.wace.2019.100219>.

## References

- Ali, H., Mishra, V., 2018. Contributions of dynamic and thermodynamic scaling in subdaily precipitation extremes in India. *Geophys. Res. Lett.* 45. <https://doi.org/10.1002/2018GL077065>.
- Bao, J., Sherwood, S.C., Alexander, L.V., Evans, J.P., 2017. Future increases in extreme precipitation exceed observed scaling rates. *Nat. Clim. Chang.* 7, 128–132. <https://doi.org/10.1038/nclimate3201>. <http://www.nature.com/doi/10.1038/nclimate3201>.



- Barbero, R., Abatzoglou, J.T., Fowler, H.J., 2018. Contribution of large-scale midlatitude disturbances to hourly precipitation extremes in the United States. *Clim. Dyn.* 0, 1–12. <https://doi.org/10.1007/s00382-018-4123-5>. <http://link.springer.com/10.1007/s00382-018-4123-5>.
- Barbero, R., Fowler, H., Lenderink, G., Blenkinsop, S., 2017. Is the intensification of precipitation extremes with global warming better detected at hourly than daily resolutions? *Geophys. Res. Lett.* 44 <https://doi.org/10.1002/2016GL071917>.
- Beck, H.E., Vergopolan, N., Pan, M., Levizzani, V., van Dijk, A.I.J.M., Weedon, G., Brocca, L., Pappenberger, F., Huffman, G.J., Wood, E.F., 2017. Global-scale evaluation of 23 precipitation datasets using gauge observations and hydrological modeling. In: *Hydrology and Earth System Sciences Discussions*, pp. 1–23. <https://doi.org/10.5194/hess-2017-508>. <https://www.hydrol-earth-syst-sci-discuss.net/hess-2017-508/>.
- Benestad, R.E., Nychka, D., Mearns, L.O., 2012. Spatially and temporally consistent prediction of heavy precipitation from mean values. *Nat. Clim. Chang.* 2, 544–547. <https://doi.org/10.1038/nclimate1497>. <https://doi.org/10.1038/nclimate1497>.
- Bennett, B., Leonard, M., Deng, Y., Westra, S., 2018. An empirical investigation into the effect of antecedent precipitation on flood volume. *J. Hydrol.* 567, 435–445. <https://doi.org/10.1016/j.jhydrol.2018.10.025>.
- Beranová, R., Kysely, J., Hanel, M., 2017. Characteristics of sub-daily precipitation extremes in observed data and regional climate model simulations. *Theor. Appl. Climatol.* 1–13. <https://doi.org/10.1007/s00704-017-2102-0>.
- Berg, P., Moseley, C., Haerter, J.O., 2013. Strong increase in convective precipitation in response to higher temperatures. *Nat. Geosci.* 6, 181–185. <https://doi.org/10.1038/ngeo1731>. <http://www.nature.com/geoindex/10.1038/ngeo1731>.
- Berghuijs, W.R., Woods, R.A., Hutton, C.J., Sivapalan, M., 2016. Dominant flood generating mechanisms across the United States. *Geophys. Res. Lett.* 43, 4382–4390. <https://doi.org/10.1002/2016GL068070>. <https://doi.org/10.1002/2016GL068070>.
- Blenkinsop, S., Fowler, H.J., Barbero, R., Chan, S.C., Guerreiro, S.B., Kendon, E., Lenderink, G., Lewis, E., Li, X.F., Westra, S., Alexander, L., Allan, R.P., Berg, P., Dunn, R.J.H., Ekström, M., Evans, J.P., Holland, G., Jones, R., Kjellström, E., Klein-Tank, A., Lettenmaier, D., Mishra, V., Prein, A.F., Sheffield, J., Tye, M.R., 2018. The INTENSE project: using observations and models to understand the past, present and future of sub-daily rainfall extremes. *Adv. Sci. Res.* 15, 117–126. <https://doi.org/10.5194/asr-15-117-2018>.
- Blenkinsop, S., Lewis, E., Chan, S.C., Fowler, H.J., 2017. Quality-control of an hourly rainfall dataset and climatology of extremes for the UK. *Int. J. Climatol.* 37, 722–740. <https://doi.org/10.1002/joc.4735>.
- Boughton, W., Jakob, D., 2017. Adjustment factors for restricted rainfall. *Aust. J. Water Resour.* 12, 37–47. <https://doi.org/10.1080/13241583.2008.11465332>.
- Brooks, H.E., Stensrud, D.J., 2000. Climatology of heavy rain events in the United States from hourly precipitation observations. *Mon. Weather Rev.* 128, 1194–1201. [https://doi.org/10.1175/1520-0493\(2000\)128<1194:COHREI>2.0.CO;2](https://doi.org/10.1175/1520-0493(2000)128<1194:COHREI>2.0.CO;2).
- Canel, L., Katz, J., 2018. Trends in U.S. Hourly precipitation variance 1949–2009. *J. Hydrometeorol.* 19, 599608. <https://doi.org/10.1175/JHM-D-17-0097.1>.
- Cortés-Hernández, V.E., Zheng, F., Evans, J.P., Lambert, M., Sharma, A., Westra, S., 2016. Evaluating regional climate models for simulating sub-daily rainfall extremes. *Clim. Dyn.* 47, 1613–1628. <https://doi.org/10.1007/s00382-015-2923-4>.
- Covey, C., Gleckler, P.J., Doutriaux, C., Williams, D.N., Dai, A., Fasullo, J., Trenberth, K., Berg, A., 2016. Metrics for the diurnal cycle of precipitation: toward routine benchmarks for climate models. *J. Clim.* 29, 4461–4471. <https://doi.org/10.1175/JCLI-D-15-0664.1>.
- Dai, A., 2001. Global precipitation and thunderstorm frequencies. Part II: diurnal variations. *J. Clim.* 1112–1128.
- Dai, A., Trenberth, K.E., 2004. The diurnal cycle and its depiction in the community climate system model. *J. Clim.* 17, 930–951. [https://doi.org/10.1175/1520-0442\(2004\)017<0930:TDCIAD>2.0.CO;2](https://doi.org/10.1175/1520-0442(2004)017<0930:TDCIAD>2.0.CO;2).
- Darwish, M., Fowler, H.J., Blenkinsop, S., Tye, M.R., 2018. A regional frequency analysis of UK hourly and multi-hourly extreme precipitation. *International Journal of Climatology In Press* 1–19. <https://doi.org/10.1002/joc.5694>.
- Davies, L., Jakob, C., May, P., Kumar, V.V., Xie, S., 2013. Relationships between the large-scale atmosphere and the small-scale convective state for Darwin, Australia. *J. Geophys. Res. Atmos.* <https://doi.org/10.1002/jgrd.50645>.
- Dee, D., Uppala, S., Simmons, a., Berrisford, P., Poli, P., Kobayashi, S., Andrae, U., Balmaseda, M., Balsamo, G., Bauer, P., 2011. The ERA - interim reanalysis: configuration and performance of the data assimilation system. *Quarterly Journal of the Royal Meteorological Society*. <https://doi.org/10.1002/qj.828>.
- Donat, M.G., Lowry, A.L., Alexander, L.V., O’Gorman, P.A., Maher, N., 2017. Addendum: more extreme precipitation in the world’s dry and wet regions. *Nat. Clim. Chang.* 7, 154–158. <https://doi.org/10.1038/nclimate3160>. <http://www.nature.com/doi/10.1038/nclimate3160>.
- Dong, W., Lin, Y., Wright, J.S., Xie, Y., Yin, X., Guo, J., 2018. Precipitable water and CAPE dependence of rainfall intensities in China. *Clim. Dyn.* 0, 0. <https://doi.org/10.1007/s00382-018-4327-8>. <https://doi.org/10.1007/s00382-018-4327-8>.
- Doswell, C.A., Brooks, H.E., Maddox, R.A., 1996. Flash flood forecasting: an ingredients-based methodology. *Weather Forecast.* 11, 560–581. [https://doi.org/10.1175/1520-0434\(1996\)011<0560:FFFAIB>2.0.CO;2](https://doi.org/10.1175/1520-0434(1996)011<0560:FFFAIB>2.0.CO;2). [http://journals.ametsoc.org/doi/abs/10.1175/1520-0434\(1996\)011<0560:FFFAIB>2.0.CO;2](http://journals.ametsoc.org/doi/abs/10.1175/1520-0434(1996)011<0560:FFFAIB>2.0.CO;2).
- Evans, J.P., Westra, S., 2012. Investigating the mechanisms of diurnal rainfall variability using a regional climate model. *J. Clim.* 25, 7232–7247. <https://doi.org/10.1175/JCLI-D-11-00616.1>.
- Feng, Z., Dong, X., Xi, B., McFarlane, S.A., Kennedy, A., Lin, B., Minnis, P., 2012. Life cycle of midlatitude deep convective systems in a Lagrangian framework. *J. Geophys. Res. Atmos.* 117, 1–14. <https://doi.org/10.1029/2012JD018362>.
- Fosser, G., Khodayar, S., Berg, P., 2014. Benefit of convection permitting climate model simulations in the representation of convective precipitation. *Clim. Dyn.* 44, 45–60. <https://doi.org/10.1007/s00382-014-2242-1>.
- Garreaud, R.D., Wallace, J.M., 1997. The diurnal March of convective cloudiness over the Americas. *Mon. Weather Rev.* 125, 3157–3171. [https://doi.org/10.1175/1520-0493\(1997\)125<3157:TDMOCC>2.0.CO;2](https://doi.org/10.1175/1520-0493(1997)125<3157:TDMOCC>2.0.CO;2).
- Groisman, P.Y., Knight, R.W., Karl, T.R., 2012. Changes in intense precipitation over the Central United States. *J. Hydrometeorol.* 13, 47–66. <https://doi.org/10.1175/JHM-D-11-039.1>. <http://journals.ametsoc.org/doi/abs/10.1175/JHM-D-11-039.1>.
- Guerreiro, S.B., Fowler, H.J., Barbero, R., Westra, S., Lenderink, G., Blenkinsop, S., Lewis, E., Li, X.F., 2018. Detection of continental-scale intensification of hourly rainfall extremes. *Nature Climate Change*. <https://doi.org/10.1038/s41558-018-0245-3>. <http://www.nature.com/articles/s41558-018-0245-3>.
- Houze Jr., R.A., 2004. Mesoscale convective systems-review paper. *Rev. Geophys.* 42, 1–43. <https://doi.org/10.1029/2004RG000150.1>. <http://www.agu.org/pubs/crossref/2004/2004RG000150.shtml>.
- Hur, J., Raghavan, S.V., Nguyen, N.S., Liong, S.Y., 2016. Evaluation of high-resolution satellite rainfall data over Singapore. *Procedia Engineering* 154, 158–167. <https://doi.org/10.1016/j.proeng.2016.07.437>. <https://doi.org/10.1016/j.proeng.2016.07.437>.
- Ivancic, T.J., Shaw, S.B., 2016. A U.S.-based analysis of the ability of the Clausius-Clapeyron relationship to explain changes in extreme rainfall with changing temperature. *J. Geophys. Res.: Atmosphere* 121, 3066–3078. <https://doi.org/10.1002/2015JD024288>. <https://doi.org/10.1002/2015JD024288>.
- Katz, R.W., Parlange, M.B., Naveau, P., 2002. Statistics of extremes in hydrology. *Adv. Water Resour.* [https://doi.org/10.1016/S0309-1708\(02\)00056-8](https://doi.org/10.1016/S0309-1708(02)00056-8).
- Kendon, E.J., Ban, N., Roberts, N.M., Fowler, H.J., Roberts, M.J., Chan, S.C., Evans, J.P., Fosser, G., Wilkinson, J.M., 2017. Do convection-permitting regional climate models improve projections of future precipitation change? *Bull. Am. Meteorol. Soc.* <https://doi.org/10.1175/BAMS-D-15-0004.1>.
- Kendon, E.J., Blenkinsop, S., Fowler, H.J., 2018. When will we detect changes in short-duration precipitation extremes? *J. Clim.* <https://doi.org/10.1175/JCLI-D-17-0435.1>.
- Kendon, E.J., Roberts, N.M., Senior, C.A., Roberts, M.J., 2012. Realism of rainfall in a very high-resolution regional climate model. *J. Clim.* 25, 5791–5806. <https://doi.org/10.1175/JCLI-D-11-00562.1>.
- Kikuchi, K., Wang, B., 2008. Diurnal precipitation regimes in the global tropics. *J. Clim.* 21, 2680–2696. <https://doi.org/10.1175/2007JCLI2051.1>.
- Laing, A.G., Fritsch, J.M., 1997. The global population of mesoscale convective complexes. *J. R. Meteorol. Soc.* 123, 389–405. <https://doi.org/10.1256/smsqj.53806>.
- Lamjiri, M.A., Dettinger, M.D., Ralph, F.M., Guan, B., 2017. Hourly storm characteristics along the U.S. West Coast: role of atmospheric rivers in extreme precipitation. *Geophys. Res. Lett.* 44, 7020–7028. <https://doi.org/10.1002/2017GL074193>. <https://doi.org/10.1002/2017GL074193>.
- Lenderink, G., Barbero, R., Loriaux, J., Fowler, H., 2017. Super-Clausius-Clapeyron scaling of extreme hourly convective precipitation and its relation to large-scale atmospheric conditions. *J. Clim.* 30 <https://doi.org/10.1175/JCLI-D-16-0808.1>.
- Lenderink, G., van Meijgaard, E., 2008. Increase in hourly precipitation extremes beyond expectations from temperature changes. *Nat. Geosci.* 1, 511–514. <https://doi.org/10.1038/ngeo262>. <http://www.nature.com/doi/10.1038/ngeo262>.
- Lepore, C., Allen, J.T., Tippet, M.K., 2016. Relationships between hourly rainfall intensity and atmospheric variables over the contiguous United States. *J. Clim.* <https://doi.org/10.1175/JCLI-D-15-0331.1>.
- Lepore, C., Veneziano, D., Molini, A., 2015. Temperature and CAPE dependence of rainfall extremes in the eastern United States. *Geophys. Res. Lett.* 42, 74–83. <https://doi.org/10.1002/2014GL062247>.
- Lewis, E., Fowler, H.J., Alexander, L., Dunn, R., McClean, F., Barbero, R., Guerreiro, S., Li, X.F., Blenkinsop, S., 2019. GSDR: a global sub-daily rainfall dataset. *J. Clim.* 32, 47154729. <https://doi.org/10.1175/JCLI-D-18-0143.1>.
- Li, J., 2017. Hourly station-based precipitation characteristics over the Tibetan Plateau. *Int. J. Climatol.* <https://doi.org/10.1002/joc.5281>. <https://doi.org/10.1002/2017GL074193>.
- Lochbihler, K., Lenderink, G., Siebesma, A.P., 2017. The spatial extent of rainfall events and its relation to precipitation scaling. *Geophys. Res. Lett.* <https://doi.org/10.1002/2017GL074857>. <https://doi.org/10.1002/2017GL074857>.
- Loriaux, J.M., Lenderink, G., Pier Siebesma, A., 2017. Large-scale controls on extreme precipitation. *J. Clim.* 30, 955–968. <https://doi.org/10.1175/JCLI-D-16-0381.1>.
- Luo, Y., Wu, M., Ren, F., Li, J., Wong, W.K., 2016. Synoptic situations of extreme hourly precipitation over China. *J. Clim.* 29, 8703–8719. <https://doi.org/10.1175/JCLI-D-16-0057.1>.
- Masaki, Y., Hanasaki, N., Takahashi, K., Hijioka, Y., 2014. Global-scale analysis on future changes in flow regimes using Gini and Lorenz asymmetry coefficients. *Water Resour. Res.* <https://doi.org/10.1002/2013WR014266>.
- McCorkle, T.A., Williams, S.S., Pfeiffer, T.A., Basara, J.B., 2016. Atmospheric contributors to heavy rainfall events in the Arkansas-red river basin. *Advances in Meteorology*. <https://doi.org/10.1155/2016/4597912>.
- Mooney, P.A., Broderick, C., Bruyère, C.L., Mulligan, F.J., Prein, A.F., 2017. Clustering of observed diurnal cycles of precipitation over the United States for evaluation of a WRF multiphysics regional climate ensemble. *J. Clim.* 30, 9267–9286. <https://doi.org/10.1175/JCLI-D-16-0851.1>.
- Morbiddelli, R., Saltalippi, C., Flammini, A., Cifrodelli, M., Picciafuoco, T., Corradini, C., Casas-Castillo, M.C., Fowler, H.J., Wilkinson, S.M., 2017. Effect of temporal aggregation on the estimate of annual maximum rainfall depths for the design of hydraulic infrastructure systems. *J. Hydrol.* 554, 710–720. <https://doi.org/10.1016/j.jhydrol.2017.09.050>. <https://doi.org/10.1016/j.jhydrol.2017.09.050>.



- Morbidelli, R., Saltalippi, C., Flammini, A., Corradini, C., Wilkinson, S.M., Fowler, H.J., 2018. Influence of temporal data aggregation on trend estimation for intense rainfall. *Adv. Water Resour.* 122, 304–316. <https://doi.org/10.1016/j.advwatres.2018.10.027>. <https://linkinghub.elsevier.com/retrieve/pii/S030917081830397X>.
- Moron, V., Barbero, R., Evans, J.P., Westra, S., Fowler, H.J., 2019. Weather types and hourly to multi-day rainfall characteristics in Tropical Australia. *J. Clim.* 32, 39834011. <http://journals.ametsoc.org/doi/10.1175/JCLI-D-18-0384.1>. <https://doi.org/10.1175/JCLI-D-18-0384.1>.
- Moseley, C., Hohenegger, C., Berg, P., Haerter, J.O., 2016. Intensification of convective extremes driven by cloud-cloud interaction. *Nat. Geosci.* <https://doi.org/10.1038/ngeo2789>.
- Pendergrass, A.G., Knutti, R., 2018. The uneven nature of daily precipitation and its change. *Geophys. Res. Lett.* 1–9. <https://doi.org/10.1029/2018GL080298>. <https://doi.org/10.1029/2018GL080298>.
- Pfahl, S., O’Gorman, P.A., Fischer, E.M., 2017. Understanding the regional pattern of projected future changes in extreme precipitation. *Nat. Clim. Chang.* 7, 423–427. <https://doi.org/10.1038/nclimate3287>. <http://www.nature.com/doi/10.1038/nclimate3287>.
- Ploshay, J.J., Lau, N.C., 2010. Simulation of the diurnal cycle in tropical rainfall and circulation during boreal summer with a high-resolution GCM. *Mon. Weather Rev.* 138, 3434–3453. <https://doi.org/10.1175/2010MWR3291.1>. <http://journals.ametsoc.org/doi/abs/10.1175/2010MWR3291.1>.
- Prein, A.F., Langhans, W., Fosser, G., Ferrone, A., Ban, N., Goergen, K., Keller, M., Tölle, M., Gutjahr, O., Feser, F., Brisson, E., Kollet, S., Schmidli, J., Van Lipzig, N.P., Leung, R., 2015. A review on regional convection-permitting climate modeling: demonstrations, prospects, and challenges. *Rev. Geophys.* 53, 323–361. <https://doi.org/10.1002/2014RG000475>.
- Prein, A.F., Liu, C., Ikeda, K., Bullock, R., Rasmussen, R.M., Holland, G.J., Clark, M., 2017. Simulating North American mesoscale convective systems with a convection-permitting climate model. *Clim. Dyn.* <https://doi.org/10.1007/s00382-017-3993-2>. <http://link.springer.com/10.1007/s00382-017-3993-2>.
- Prein, A.F., Liu, C., Ikeda, K., Trier, S.B., Rasmussen, R.M., Holland, G.J., Clark, M.P., 2017. Increased rainfall volume from future convective storms in the US. *Nat. Clim. Chang.* 1–7. <https://doi.org/10.1038/s41558-017-0007-7>. <https://doi.org/10.1038/s41558-017-0007-7>.
- Prein, A.F., Rasmussen, R.M., Ikeda, K., Liu, C., Clark, M.P., Holland, G.J., 2016. The future intensification of hourly precipitation extremes. *Nat. Clim. Chang.* 7, 48–52. <https://doi.org/10.1038/nclimate3168>. <http://www.nature.com/doi/10.1038/nclimate3168>.
- Rajah, K., O’Leary, T., Turner, A., Petrakis, G., Leonard, M., Westra, S., 2014. Changes to the temporal distribution of daily precipitation. *Geophys. Res. Lett.* 41 <https://doi.org/10.1002/2014GL062156>.
- Rutledge, S.A., Williams, E.R., Keenan, T.D., 2002. The down upper Doppler and electricity experiment (DUNDEE): overview and preliminary results. *Bull. Am. Meteorol. Soc.* [https://doi.org/10.1175/1520-0477\(1992\)073<0003:tdudae>2.0.co;2](https://doi.org/10.1175/1520-0477(1992)073<0003:tdudae>2.0.co;2).
- Rutz, J.J., Steenburgh, W.J., Ralph, F.M., 2014. Climatological characteristics of atmospheric rivers and their inland penetration over the western United States. *Mon. Weather Rev.* <https://doi.org/10.1175/MWR-D-13-00168.1>.
- Schroeder, K., Kirchengast, G., 2017. Sensitivity of extreme precipitation to temperature: the variability of scaling factors from a regional to local perspective. *Clim. Dyn.* <https://doi.org/10.1007/s00382-017-3857-9>, 0, 0. <http://link.springer.com/10.1007/s00382-017-3857-9>.
- Sippel, S., Zscheischler, J., Heimann, M., Lange, H., Mahecha, M.D., Jan Van Oldenborgh, G., Otto, F.E., Reichstein, M., 2017. Have precipitation extremes and annual totals been increasing in the world’s dry regions over the last 60 years? *Hydrol. Earth Syst. Sci.* 21, 441–458. <https://doi.org/10.5194/hess-21-441-2017>.
- Syafrina, A.H., Zalina, M.D., Juneng, L., 2015. Historical trend of hourly extreme rainfall in Peninsular Malaysia. *Theor. Appl. Climatol.* <https://doi.org/10.1007/s00704-014-1145-8>.
- Trenberth, K.E., Dai, A., Rasmussen, R.M., Parsons, D.B., 2003. The changing character of precipitation. *Bull. Am. Meteorol. Soc.* 84, 1205–1217. <https://doi.org/10.1175/BAMS-84-9-1205>.
- Trenberth, K.E., Zhang, Y., Gehne, M., 2017. Intermittency in precipitation: duration, frequency, intensity, and amounts using hourly data. *J. Hydrometeorol.* 18, 1393–1412. <https://doi.org/10.1175/JHM-D-16-0263.1>. <http://journals.ametsoc.org/doi/10.1175/JHM-D-16-0263.1>.
- Utsumi, N., Kim, H., Kanae, S., Oki, T., 2017. Relative contributions of weather systems to mean and extreme global precipitation. *J. Geophys. Res.: Atmosphere* 122, 152–167. <https://doi.org/10.1002/2016JD025222>. <https://doi.org/10.1002/2016JD025222>.
- Utsumi, N., Seto, S., Kanae, S., Maeda, E.E., Oki, T., 2011. Does higher surface temperature intensify extreme precipitation? *Geophys. Res. Lett.* 38, 1–5. <https://doi.org/10.1029/2011GL048426>.
- Villarini, G., 2016. On the seasonality of flooding across the continental United States. *Adv. Water Resour.* 87, 80–91. <https://doi.org/10.1016/j.advwatres.2015.11.009>. <https://doi.org/10.1016/j.advwatres.2015.11.009>.
- Westra, S., Alexander, L.V., Zwiers, F.W., 2013. Global increasing trends in annual maximum daily precipitation. *J. Clim.* 26, 3904–3918. <https://doi.org/10.1175/JCLI-D-12-00502.1>.
- Westra, S., Fowler, H.J., Evans, J.P., Alexander, L.V., Berg, P., Johnson, F., Kendon, E.J., Lenderink, G., Roberts, N.M., 2014. Future changes to the intensity and frequency of short-duration extreme rainfall. *Rev. Geophys.* 52, 522–555. <https://doi.org/10.1002/2014RG000464>. <https://doi.org/10.1002/2014RG000464>.
- Westra, S., Sisson, S.A., 2011. Detection of non-stationarity in precipitation extremes using a max-stable process model. *J. Hydrol.* 406, 119–128. <https://doi.org/10.1016/j.jhydrol.2011.06.014>. <https://doi.org/10.1016/j.jhydrol.2011.06.014>.
- Wu, Y., Huang, A., Huang, D., Chen, F., Yang, B., Zhou, Y., Fang, D., Zhang, L., Wen, L., 2017. Diurnal variations of summer precipitation over the regions east to Tibetan Plateau. *Clim. Dyn.* 0, 0. <https://doi.org/10.1007/s00382-017-4042-x>. <http://link.springer.com/10.1007/s00382-017-4042-x>.
- Wu, Y., Raman, S., 1998. The summertime Great Plains low level jet and the effect of its origin on moisture transport. *Boundary-Layer Meteorol.* 88, 445–466. <https://doi.org/10.1023/A:1001518302649>.
- Xiao, C., Wu, P., Zhang, L., Song, L., 2016. Robust increase in extreme summer rainfall intensity during the past four decades observed in China. *Sci. Rep.* 6, 38506. <https://doi.org/10.1038/srep38506>. <http://www.nature.com/articles/srep38506>.
- Xiao, C., Yuan, W., Yu, R., 2018. Diurnal cycle of rainfall in amount, frequency, intensity, duration, and the seasonality over the UK. *Int. J. Climatol.* 1–12. <https://doi.org/10.1002/joc.5790>. <https://doi.org/10.1002/joc.5790>.
- Yuan, W., Yu, R., Zhang, M., Lin, W., Li, J., Fu, Y., 2013. Diurnal cycle of summer precipitation over subtropical East Asia in CAM5. *J. Clim.* 26, 3159–3172. <https://doi.org/10.1175/JCLI-D-12-00119.1>.
- Zhang, X., Zwiers, F.W., Li, G., Wan, H., Cannon, A.J., 2017. Complexity in estimating past and future extreme short-duration rainfall. *Nat. Geosci.* 10, 255–259. <https://doi.org/10.1038/ngeo2911>. <http://www.nature.com/doi/10.1038/ngeo2911>.
- Zheng, F., Westra, S., Leonard, M., 2015. Opposing local precipitation extremes. *Nat. Clim. Chang.* 5, 389–390. <https://doi.org/10.1038/nclimate2579>. <http://www.nature.com/doi/10.1038/nclimate2579>.